J. Fluid Mech. (2006), *vol.* 559, *pp.* 117–149.
doi:10.1017/S0022112006000164 Printed in the United Kingdom

Evaluations of the von Kármán constant in the atmospheric surface layer

By EDGAR L ANDREAS[1], KERRY J. CLAFFEY[1], RACHEL E. JORDAN[1], CHRISTOPHER W. FAIRALL[2], PETER S. GUEST[3], P. OLA G. PERSSON[2,4] AND ANDREY A. GRACHEV[2,4]

[1]US Army Cold Regions Research and Engineering Laboratory, Hanover, NH 03755, USA
[2]NOAA Earth System Research Laboratory, Physical Sciences Division, Boulder, CO 80305, USA
[3]Naval Postgraduate School, Monterey, CA 93943, USA
[4]Cooperative Institute for Research in Environmental Sciences, University of Colorado, Boulder, CO 80309, USA

(Received 7 February 2005 and in revised form 14 December 2005)

The von Kármán constant k relates the flow speed profile in a wall-bounded shear flow to the stress at the surface. Recent laboratory studies in aerodynamically smooth flow report k values that cluster around 0.42–0.43 *and* around 0.37–0.39. Recent data from the atmospheric boundary layer, where the flow is usually aerodynamically rough, are similarly ambiguous: k is often reported to be significantly smaller than the canonical value 0.40, and two recent data sets suggest that k decreases with increasing roughness Reynolds number Re_*. To this discussion, we bring two large atmospheric data sets that suggest k is constant, 0.387 ± 0.003, for $2 \leqslant Re_* \leqslant 100$.

The data come from our yearlong deployment on Arctic sea ice during SHEBA, the experiment to study the Surface Heat Budget of the Arctic Ocean, and from over 800 h of observations over Antarctic sea ice on Ice Station Weddell (ISW). These were superb sites for atmospheric boundary-layer research; they were horizontally homogeneous, uncomplicated by topography, and unobstructed and uniform for hundreds of kilometres in all directions.

During SHEBA, we instrumented a 20 m tower at five levels between 2 and 18 m with identical sonic anemometer/thermometers and, with these, measured hourly averaged values of the wind speed $U(z)$ and the stress $\tau(z)$ at each tower level z. On ISW, we measured the wind-speed profile with propeller anemometers at four heights between 0.5 and 4 m and measured τ with a sonic anemometer/thermometer at one height. On invoking strict quality controls, we gleaned 453 hourly $U(z)$ profiles from the SHEBA set and 100 from the ISW set. All of these profiles reflect near-neutral stratification, and each exhibits a logarithmic layer that extends over all sampling heights. By combining these profiles and our measurements of τ, we made 553 independent determinations of k. This is, thus, the largest, most comprehensive atmospheric data set ever used to evaluate the von Kármán constant.

1. Introduction

The Kansas experiment focused attention in the atmospheric boundary-layer community on the crucial role that the von Kármán constant k plays in boundary-layer theory. In reporting that $k = 0.35$, Businger *et al.* (1971) created a firestorm of

uncertainty and, in fact, produced a division in the community: one camp immediately embraced the new value for its analyses; and the other camp stuck with the traditional value of 0.40–0.41. Although Wieringa (1980) later eased the apprehensions of some by arguing that flow distortion explained the small Kansas k value and by then suggesting that the corrected Kansas result should be $k = 0.41$, Wyngaard *et al.* (1982) were unconvinced and stood by their value of 0.35.

Several other atmospheric scientists addressed this controversy with reviews and theory. For example, after reviewing Tennekes's (1968) theory, which predicts $k = 0.33$ for very large Reynolds numbers, Yaglom (1974) concluded that k is known only with an error of about 20 % and that no basis exists to reject the hypothesis that $k = 0.4$ ('without the second decimal place'). Using a model for boundary-layer plumes and downdrafts, Telford (1982) predicted $k = 0.37$. Coincidentally, using renormalization-group analysis, though not applying it necessarily in the atmosphere, Yakhot & Orszag (1986*a*, *b*) also obtained the same theoretical value, 0.37. Tennekes (1973) used similarity arguments to suggest that, in the atmosphere, k should become constant only as the Rossby number approaches infinity. However, Högström (1996) saw no Rossby number influence on k in his review of 18 atmospheric data sets.

As interest in measuring k in the atmosphere intensified, more and more frequently was it reported to be less than 0.40. From among the several sets of such measurements, we mention as examples the values of Francey & Garratt (1981), 0.33 ± 0.03 and 0.38 ± 0.04 depending on the stratification correction they used; Dyer & Bradley (1982), 0.385 ± 0.021; and Kondo & Sato (1982), 0.39. In another set of measurements with large Reynolds number – though in a laboratory wind-wave tunnel – Tseng, Hsu & Wu (1992) obtained $k = 0.37 \pm 0.03$. Similarly, Telford & Businger (1986) reinterpreted data reported by Högström (1985) and concluded that these suggest $k = 0.359 \pm 0.014$ rather than the 0.400 ± 0.011 that Högström obtained.

Based on 29 data points from the atmospheric surface layer, Frenzen & Vogel (1995*a*) reported k to be 0.39 ± 1 % but later revised this value to 0.387 ± 0.010 (Frenzen & Vogel 1995*b*). Similarly, from roughly a hundred data points from both their own measurements and historical sets, Oncley *et al.* (1996) obtained an average value for k of 0.365 ± 0.015. More importantly, though, these three papers suggest that k decreases weakly with increasing roughness Reynolds number (see also Vogel & Frenzen 2002).

In his extensive review of atmospheric observations, Högström (1996) concluded that 'k is actually constant in atmospheric surface-layer flow, having in fact the same value as is found from laboratory data', 0.40, regardless of whether the flow is aerodynamically smooth or rough. The irony here is that, shortly after Högström published his paper, several studies appeared to contradict the notion that laboratory measurements agree that k is 0.40. First, Zagarola & Smits (1998) published highly regarded measurements of the von Kármán constant at large Reynolds number in the Princeton superpipe. Their conclusion was that $k = 0.436 \pm 0.002$ in aerodynamically smooth flow. Perry, Hafez & Chong (2001), however, reanalysed these pipe data and interpreted them to give $k = 0.39$; but, McKeon (2003) suggested some possible biases in the analysis by Perry *et al.* that would result in k values that were biased low. Then, using new corrections for the Pitot tubes used to measure the velocity profile, McKeon *et al.* (2004) reanalysed the Zagarola & Smits data and also obtained new data in the Princeton superpipe. Their analysis of these two data sets yielded $k = 0.421 \pm 0.002$, thereby corroborating the larger value in aerodynamically smooth flow that Zagarola & Smits found.

In contrast, though, Zanoun, Durst & Nagib (2003) made measurements in aerodynamically smooth high-Reynolds-number flow in a wind tunnel that yielded $k = 0.37$, which they note is approximately e^{-1}. Likewise, Österlund *et al.* (2000) reported measurement from wind tunnels at the Royal Institute of Technology in Stockholm and at Illinois Institute of Technology (IIT) that yielded $k = 0.38$ in aerodynamically smooth flow. The key feature of both of their data sets is that the wind tunnels had zero pressure gradient. Nagib, Christophorou & Monkewitz (2004) obtained several new velocity profile data sets from the IIT wind tunnel with a different pressure gradient along the tunnel for each set. Again, for measurements with zero pressure gradient, they found $k = 0.38$. However, we infer from their measurements in favourable and adverse pressure gradients that their analysis technique would yield k values that are biased low for an adverse pressure gradient and are biased high for a favourable pressure gradient. Coincidentally, the Princeton superpipe had a favourable pressure gradient for the data sets that Zagarola & Smits (1998) and McKeon *et al.* (2004) reported.

In summary, the best recent laboratory results no longer support the canonical laboratory value of $k = 0.40$ that Högström (1996) advocated; but the field is again divided, at least for aerodynamically smooth flow. Some laboratory data suggest that k is significantly larger than 0.40, while other laboratory data suggest k is smaller than 0.40. The two results may arise as a consequence of the presence or absence of a pressure gradient in the laboratory flows. Meanwhile, in the atmospheric surface layer, where the flow is commonly aerodynamically rough and the along-wind pressure gradient is very small, k seems to be smaller than 0.40.

Here we bring to this discussion the two largest data sets ever obtained in the atmospheric surface layer that have implications for understanding the behaviour of the von Kármán constant. We collected these data over sea ice during SHEBA, the experiment to study the Surface Heat Budget of the Arctic Ocean (Andreas *et al.* 1999; Persson *et al.* 2002; Uttal *et al.* 2002), and in the Antarctic on Ice Station Weddell (ISW; Gordon & Lukin 1992; ISW Group 1993).

In the next section, we review the logarithmic flow speed profile for both aerodynamically smooth and aerodynamically rough flow. This discussion highlights that the roughness Reynolds number is an important dynamic parameter for characterizing wall-bounded shear flows. After next describing our SHEBA and Ice Station Weddell data, we demonstrate that the logarithmic wind speed profile is quite robust; it appears routinely in the atmospheric surface layer in near-neutral stratification even when the stress is not constant with height.

From the logarithmic wind speed profiles and our SHEBA and ISW measurements of the friction velocity u_*, we make 553 independent evaluations of the von Kármán constant. At first sight, these seem to vary dramatically with roughness Reynolds number Re_*, approaching the constant value of 0.421 found by McKeon *et al.* (2004) in aerodynamically smooth flow but decreasing to levels as low as 0.30 for $Re_* \geqslant 200$. After further analyses, we suggest that measurement uncertainty explains the spread in k values; and artificial correlation that results from the shared variables that go into evaluating k and defining Re_* explains the apparent Reynolds number dependence of k. We corroborate this latter conclusion by demonstrating that our k values are uncorrelated with values of Re_* computed with a bulk flux algorithm that does not use any variables shared with k. We thus conclude that the von Kármán constant is, indeed, constant and has a value of 0.387 ± 0.003 for roughness Reynolds numbers between 2 and 100.

2. The logarithmic wind speed profile

The logarithmic flow speed profile is a very robust experimental and mathematical feature of wall-bounded shear flows. Classically, that profile derives from mixing length arguments (e.g. Goldstein 1965, p. 208ff.; Schlichting 1968, p. 545ff.; Hinze 1975, p. 624ff.). In a neutrally stratified atmospheric surface layer where only one length scale – the distance z above the surface – characterizes the flow, these arguments still work (e.g. Businger 1973; Fleagle & Businger 1980, p. 272ff.); but in the atmosphere, asymptotic similarity arguments, as developed by Blackadar & Tennekes (1968) and Tennekes (1973; see also Garratt 1992), yield an elegant and less constrained derivation of the logarithmic wind speed profile.

In essence, all of these varied analyses predict that the surface stress τ_0 is related to the vertical profile of the longitudinal wind speed, $U(z)$, through

$$\tau_0 = \rho\, u_{*0} k z \frac{\partial U}{\partial z}. \tag{2.1}$$

Here, $\tau_0 = -\rho\overline{uw}_0$, where ρ is the air density, u and w are turbulent velocity fluctuations in the along-wind and vertical directions, and the overbar indicates a time average. Also in (2.1), $u_{*0} \equiv (\tau_0/\rho)^{1/2}$ is the friction velocity, and k is the von Kármán constant. That is, the von Kármán relates the surface stress to the near-surface flow speed profile. Because $\tau_0 = \rho u_{*0}^2$, (2.1) reduces to

$$\frac{u_{*0}}{kz} = \frac{\partial U}{\partial z}. \tag{2.2}$$

For flow over an aerodynamically smooth surface, ν/u_{*0}, where ν is the kinematic viscosity, is the only available length scale with which to non-dimensionalize (2.2). Equation (2.2) thus becomes

$$\frac{1}{kz_+} = \frac{\partial(U/u_{*0})}{\partial z_+}, \tag{2.3}$$

where $z_+ = u_{*0} z/\nu$. This has the solution

$$\frac{U(z)}{u_{*0}} = \frac{1}{k} \ln\left(\frac{u_{*0} z}{\nu}\right) + B, \tag{2.4}$$

where B is an integration constant that must be found experimentally.

On the other hand, for flow that is aerodynamically rough or in transition between smooth and rough, the aerodynamic roughness length z_0 can non-dimensionalize (2.2). Thus,

$$\frac{1}{k\xi} = \frac{\partial(U/u_{*0})}{\partial \xi}, \tag{2.5}$$

where $\xi = z/z_0$. Equation (2.5) has the solution

$$\frac{U(z)}{u_{*0}} = \frac{1}{k} \ln\left(\frac{z}{z_0}\right), \tag{2.6}$$

which has no additive integration constant because z_0 is defined such that $U(z) = 0$ at $z = z_0$.

Because the length scales ν/u_{*0} and z_0 characterize aerodynamically smooth and aerodynamically rough flow, their ratio $Re_* \equiv u_{*0} z_0/\nu$, the roughness Reynolds number, is dynamically important. One of our purposes here is to investigate the suggestion that the von Kármán constant depends on Re_*.

On comparing (2.4) and (2.6), we can define a roughness length for aerodynamically smooth flow, z_{0s}, that has the same property as does z_0; the wind speed profile is zero for $z = z_{0s}$. This parameter is (e.g. Monin & Yaglom 1971, p. 287; Andreas & Treviño 2000)

$$z_{0s} = (\nu/u_{*0}) \exp(-k\,B). \tag{2.7}$$

With typical values for k and B of 0.4 and 5 (Tennekes & Lumley 1972, p. 157; Yaglom 1993; Long, Wiberg & Nowell 1993),

$$z_{0s} = 0.135(\nu/u_{*0}). \tag{2.8}$$

Consequently, the roughness Reynolds number in aerodynamically smooth flow (i.e. $u_{*0}z_{0s}/\nu$) is always constant, 0.135, for the assumed values of k and B.

Aerodynamically rough flow, on the other hand, features a wide range of roughness Reynolds numbers with a minimum of about 2.5 (e.g. Schlichting 1968, p. 579ff.; Monin & Yaglom 1971, p. 288ff.; Businger 1973). Consequently, Re_* values between 0.135 and 2.5 characterize the transition region between smooth and rough flow.

3. Measurements

3.1. *During SHEBA*

The experiment to study the Surface Heat Budget of the Arctic Ocean (SHEBA) centred on an ice camp in the Beaufort Gyre of the Arctic Ocean. Uttal *et al.* (2002) show the drift track of this camp, which was manned continuously from 2 October 1997 until 11 October 1998.

Throughout this experiment, we maintained a 20 m meteorological tower (figure 1) that was instrumented at five levels with identical three-axis sonic anemometer/thermometers (Applied Technologies, Longmont, Colorado). The tower had two sections: a 10 m tall walk-up scaffold that was 2 m on a side; and a 20 m triangular section, with each side of the triangle being about 0.5 m.

We mounted three sonics on the scaffold at the ends of booms that extended about 3 m from the scaffold. The triangular section had two instrument carriages: one that ran between heights of about 1 and 9 m and another that ran between 11 and 19 m. Each of these carriages held a sonic at the end of a 2 m boom. Thus, all five sonics extended at least 2 m in front of our open tower; we therefore believe that flow distortion at the anemometers was negligible.

Although the sonics varied in height through the year over a range of about a metre as a consequence of snow accumulation and ablation (Persson *et al.* 2002, table 1), nominal heights of the three sonics on the scaffold were 3.2, 5.1 and 8.9 m. The sonic on the lower carriage of the triangular section was typically at 2.2 m; while the sonic on the upper section was, nominally, at 14 m in the winter and 18 m in the summer. Periodically, we used the carriages to move the sonics side-by-side for intercomparisons.

Our sonics were the so-called K-type, which feature three orthogonal, 15 cm sound paths that are separated to minimize flow distortion (Kaimal & Finnigan 1994, p. 218ff.). The remaining flow distortion had been studied and quantified (Kaimal *et al.* 1990); each sonic system had firmware that corrected the output for this flow distortion in real-time. The sonic output was a digital signal of the velocity measured along each of the three sonic axes and the 'sonic' temperature measured on the vertical axis. The sampling rate for each signal was 10 Hz. We logged all the raw 10 Hz data on a personal computer for later processing.

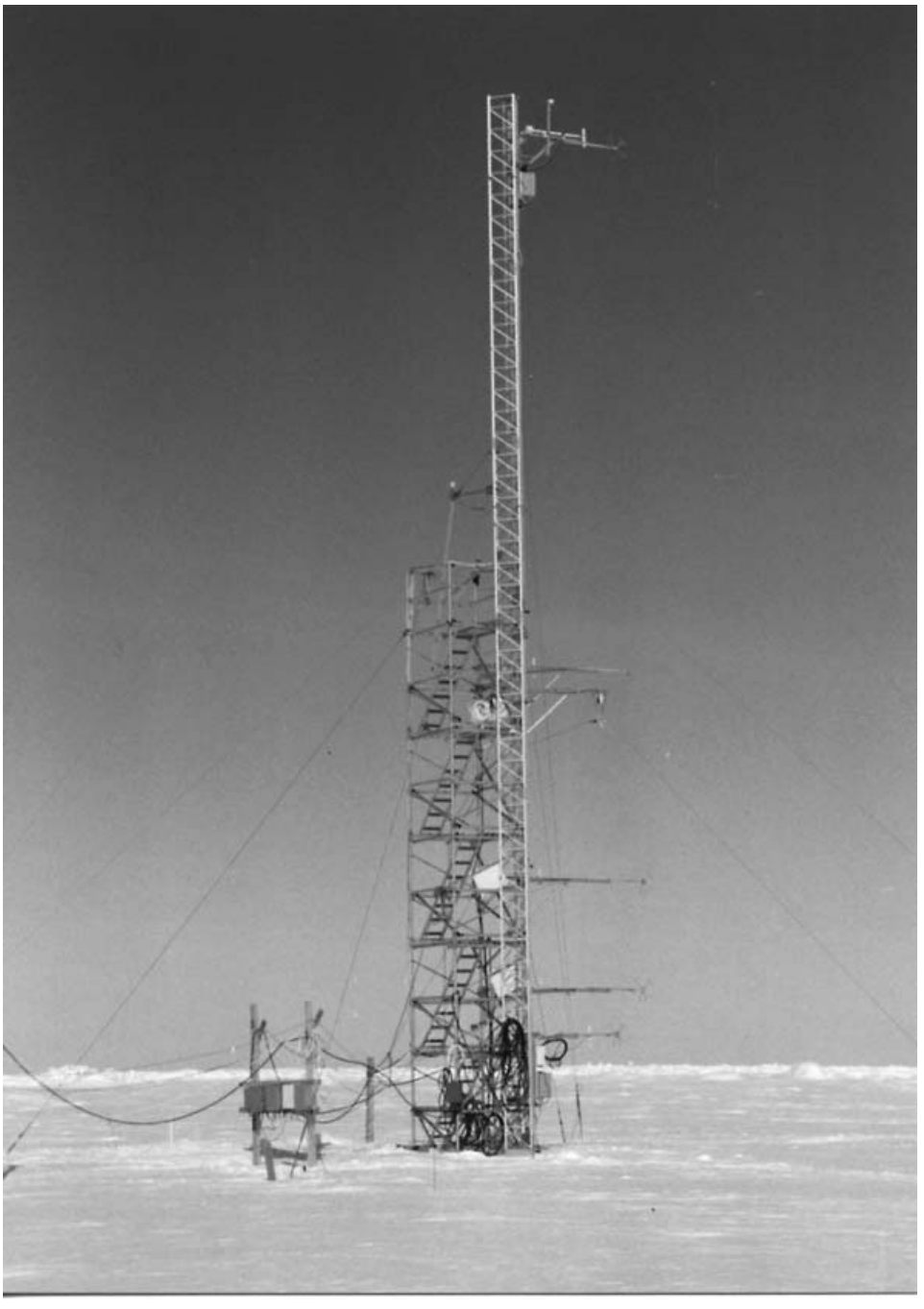

FIGURE 1. Our 20 m SHEBA tower was instrumented at five levels with identical sonic anemometer/thermometers.

Except for rare breakups of the ice camp that cut power to our site, our instruments ran almost continuously from 31 October 1997 to 29 September 1998. We averaged all variables hourly. Consequently, we potentially have over 8000 h of data for our analysis.

From our sonic anemometer/thermometers, we obtained both the mean components of the velocity vector – denoted as U, V and W, where U is along-wind, V is cross-wind, and W is vertical – and the turbulent components of velocity (u, v and w) and 'sonic' temperature (θ). As Persson *et al.* (2002) and Grachev *et al.* (2005) explain, we did spectral and cospectral analyses of these turbulent fluctuations to obtain $\overline{uw}$, the along-wind vertical stress, and $\overline{w\theta}$, the temperature flux, at each level that produced good data for the analysis hour. To obtain U, $\overline{uw}$ and $\overline{w\theta}$, we had to rotate averaged quantities from the 'sonic' frame in which they were measured to the natural 'wind' frame. We did this by requiring that the mean wind and the turbulent stress at each measurement level be in the U-direction. That is, after rotation, $V = 0$, $W = 0$ and $\overline{vw} = 0$. Hence, at each tower level with good data for the hour, we can define a mean wind speed $U(z)$ and a local stress $\tau(z)$. Although it is loose usage, as shorthand, we define a local friction velocity as $u_*(z) = [\tau(z)/\rho]^{1/2}$.

Because the sonic temperature θ is nearly the virtual temperature (Schotanus, Nieuwstadt & De Bruin 1983; Kaimal & Gaynor 1991; Larsen *et al.* 1993), our $\overline{w\theta}$ values provide a measurement of atmospheric stratification. We quantify this stratification as z/L, where L is the Obukhov length,

$$L = \left[-\frac{kg}{T_v} \frac{\overline{w\theta}}{u_*^3} \right]^{-1}. \tag{3.1}$$

Here, T_v is the average virtual temperature, and g is the acceleration due to gravity.

A common concern with sonic anemometers is that, because they average over a sound path of length d (15 cm in our case), the instruments cannot measure the smallest turbulence scales. For our K-type sonics, another concern is that the sound paths that measure u and v are separated by a distance $s = 27$ cm from the path that measures w. Hence, u and v signals lose coherence with w for the smaller turbulence scales.

Many have considered the consequences of sonic configuration on flux measurements (e.g. Moore 1986; Kristensen *et al.* 1997), but most such studies reiterate the conclusions by Kaimal, Wyngaard & Haugen (1968) that only when $\kappa_1 d > 1$ and $\kappa_1 s > 1$ are path-averaging and separation effects detrimental to sonic performance. Here, κ_1 is the one-dimensional turbulence wavenumber. In the atmospheric surface layer, we typically write $\kappa_1 = 2\pi f/U$, where f is the turbulence frequency and U is again the mean wind speed at measurement height z.

Consider the separation constraint, which is the more severe for our sonics. To ensure that our measurements of $\overline{uw}$ were unaffected by sensor separation, we must require

$$1 > \kappa_1 s = 2\pi \left(\frac{fz}{U} \right) \left(\frac{s}{z} \right). \tag{3.2}$$

Kaimal & Finnigan (1994, p. 55; cf. Kaimal *et al.* 1972) give an approximation for the non-dimensional u–w cospectrum in neutral stratification that should be a reasonable model for our measurements. We see from this model that, at a non-dimensional frequency $n \equiv fz/U = 1$, the cospectrum has fallen to 20 % of its peak value. Furthermore, if we integrate that cospectrum from $n = 0$ to $n = 1$, the result represents over 95 % of the u–w covariance. In other words, if we can sample non-dimensional frequencies up to $n = 1$, we have measured u_* to better than 97 % ($= \sqrt{0.95}$).

On substituting this result – that $fz/U = 1$ – in (3.2), we establish the measurement constraint

$$z > 2\pi s. \tag{3.3}$$

This result is a little stronger than Kristensen & Fitzjarrald's (1984) conclusion that the measurement height must be only 4–5 times the sound path for flux measurements to be unaffected by path averaging. Nevertheless, (3.3) means that our K-type sonics must be above 1.7 m for our measurements of $\overline{uw}$ to be negligibly affected by sonic geometry. All measurements at SHEBA and on Ice Station Weddell satisfied this requirement.

3.2. *On Ice Station Weddell*

Ice Station Weddell (ISW) was the first ice camp ever placed on drifting sea ice in the Antarctic for research purposes (Gordon & Lukin 1992; ISW Group 1993). It drifted northward through the western Weddell Sea from 4 February until 9 June 1992, paralleling the track of Schackleton's *Endurance*. Andreas & Claffey (1995) show the station's drift track and describe our micrometeorological measurements on ISW.

Briefly, ISW was a prologue for our longer, more comprehensive measurements at SHEBA. On ISW, we had a profiling mast instrumented with R. M. Young (Traverse City, Michigan) propeller anemometers at nominal heights of 0.5, 1, 2 and 4 m (figure 2). The lower three propellers (model 27103) had fixed orientation with respect to the mast; the highest anemometer was a propeller-vane (model 35003). These were all helicoid, four-blade 'Gill' propellers (Gill 1973). Our mast rotated, and we used the propeller-vane for reference to periodically rotate the fixed anemometers into the mean wind.

Andreas & Claffey (1995) describe these measurements in more detail, explain our quality controls, and show sample wind speed profiles obtained in near-neutral stratification. The quality-control issue that we reiterate here is that our analysis used only profiles for which the hourly averaged wind vector measured by the propeller-vane was within $\pm 20^\circ$ of being head-on to the three propellers fixed to the mast. We obtained the true wind speed from the average wind speed measured by each of these fixed propellers using the standard cosine correction, which Busch *et al.* (1980; also Wyngaard 1981; Kaimal & Finnigan 1994, p. 209ff.) show to be nearly exact for deviation angles of 20° or less.

About 20 m from the profile mast in figure 2 stood a 5 m tower with a K-type sonic anemometer/thermometer (Applied Technologies), just like the one we used at SHEBA, mounted at a height of 4.65 m. This provided hourly averages of the stress τ and the sensible heat flux $\overline{w\theta}$. Through (3.1) and our supporting meteorological measurements, this sonic also gave us the Obukhov length. Andreas, Jordan & Makshtas (2005*a*) give full details on how we logged, screened and processed these turbulence measurements on Ice Station Weddell.

We began collecting data on ISW on 25 February 1992 and ran continuously until 29 May 1992. The propeller-vane on our profile mast stopped working on 31 March, however. Without four levels in the wind-speed profile, we do not feel confident in our profile analysis. Hence, the analysis we report here goes only until 31 March, but we still have over 800 hours of data from Ice Station Weddell with which to supplement our SHEBA analysis.

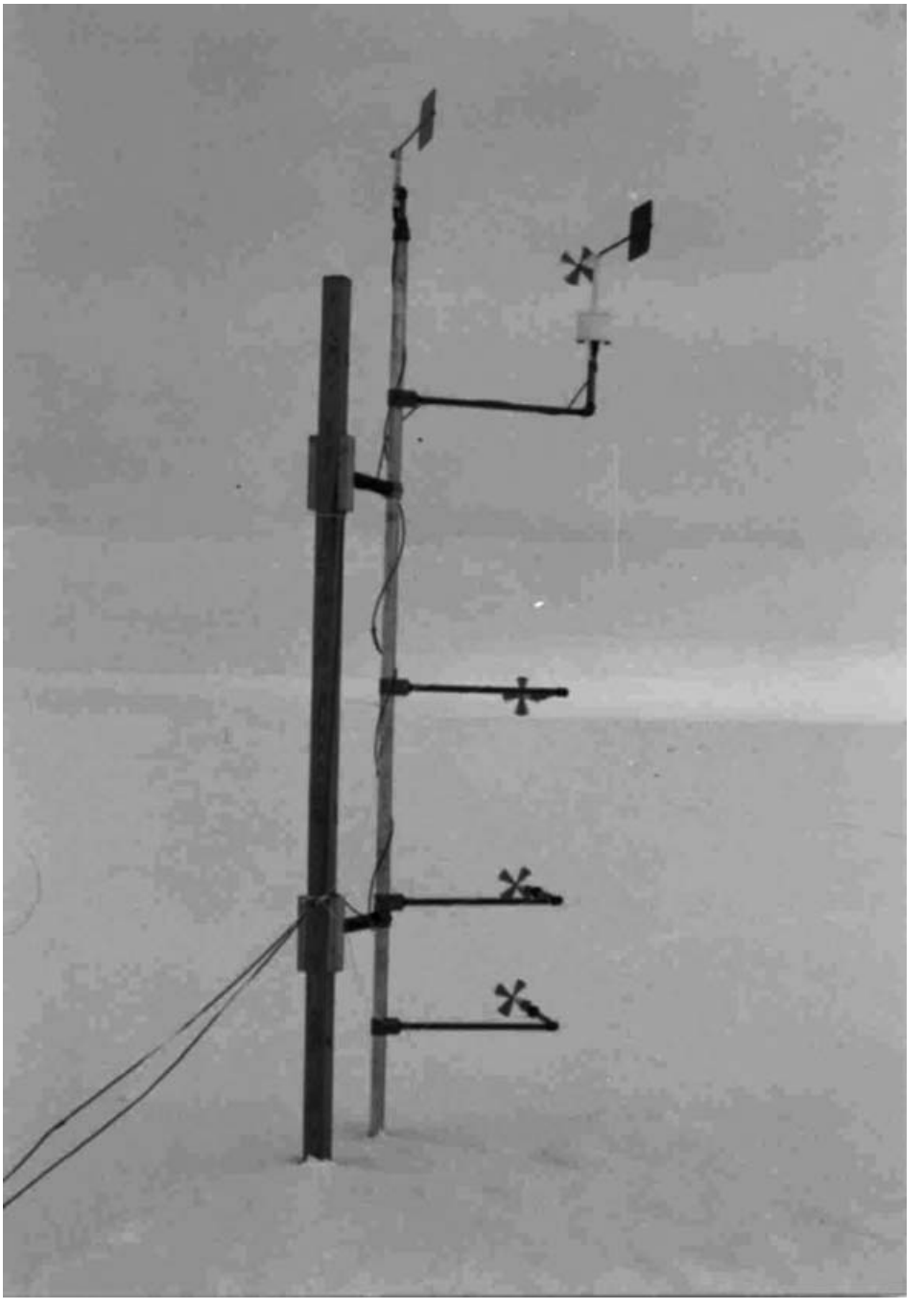

FIGURE 2. Our profile mast on Ice Station Weddell had R. M. Young propeller anemometers at four levels between 0.5 and 4 m. The upwind fetch is snow-covered sea ice.

4. Profile analysis

We analysed our SHEBA and ISW wind profile data in the context of (2.6). That is, we carried out a least-squares linear regression of $U(z)$ versus $\ln(z)$. This fitting

yielded the slope S and the intercept I such that

$$U(z) = S\ln(z) + I, \tag{4.1}$$

where we recognize

$$S = u_*/k, \tag{4.2}$$

and

$$I = -\frac{u_*}{k}\ln(z_0) = -S\ln(z_0). \tag{4.3}$$

Thus, with a measurement of u_*, (4.2) yields the von Kármán constant. In turn, with the slope S, (4.3) yields an estimate of z_0 whether the flow is aerodynamically rough, aerodynamically smooth, or in transition. We use this z_0 value in our later evaluations of Re_*.

For our SHEBA analysis, we use for u_* in (4.2) and (4.3) the inferred surface value u_{*0}. We will explain shortly how we obtained this. Since we had only one sonic anemometer on Ice Station Weddell, u_* in (4.2) and (4.3) comes from our one measurement of $(\tau/\rho)^{1/2}$ at 4.65 m.

We placed restrictions on the data to ensure that we were using only the profiles for these calculations that best met the theoretical conditions. Some of these restrictions come from Wieringa (1993) and Andreas & Claffey (1995).

4.1. *Quality controls*

First, to ensure the most accurate estimates of S and I, we excluded any hours from our SHEBA set that did not have good data for both $U(z)$ and $\tau(z)$ for all five tower levels. For the Ice Station Weddell set, we required that τ and all four $U(z)$ levels be available.

Secondly, (4.1) is strictly valid only for neutral stratification. Our first screening for neutral stratification was to analyse only profiles for which the wind speed at all levels was at least $4\,\mathrm{m\,s^{-1}}$. In laboratory flows, the walls of the channel impose a longitudinal direction on the flow, even at very low flow speeds. In the atmospheric boundary layer, in contrast, turbulence statistics in low wind speeds are very difficult to measure because the wind is often directionally unstable (e.g. Andreas *et al.* 1998). Velocity covariances are, thus, poorly defined, as are the angles for the required coordinate rotations (Mahrt 1998). Requiring wind speeds of at least $4\,\mathrm{m\,s^{-1}}$ eliminates most such meandering flows from our analysis and, in effect, also tends to eliminate non-stationary conditions.

Our third condition involved the upwind fetch. The SHEBA ice camp was centred around the Canadian icebreaker *Des Groseilliers*. When we originally built the camp, we placed our 20 m tower at the north end with the *Des Groseilliers* and all other camp structures in a 75° sector south of the tower. In this configuration, the undisturbed sector that our tower instruments could sample without flow through the tower itself or over other structures in the camp was approximately 280°. During the course of our SHEBA deployment, however, our undisturbed sector narrowed somewhat because the sea ice moved and deformed. We tracked these changes in fetch conditions and, for our analyses, rejected any profiles for which the winds were coming from any sectors containing camp structures.

The undisturbed sector at SHEBA had a natural sea ice surface for untold hundreds of kilometres. This was snow-covered from the beginning of the experiment until roughly 1 June 1998, when the snow began to melt. All the snow had melted by early July, and melt ponds formed and grew to cover about 20 % of the surface by mid-July. The ponds had refrozen by mid-August, and snow began accumulating again on the

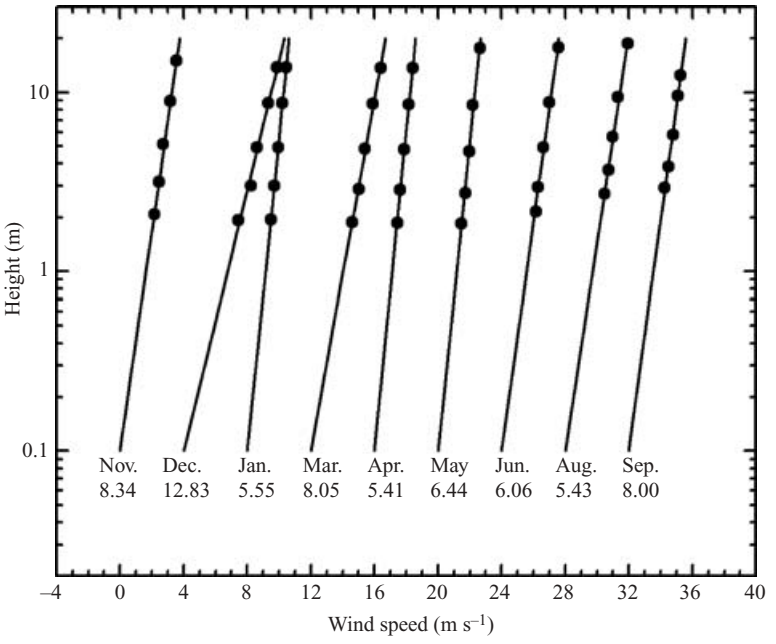

FIGURE 3. Representative logarithmic wind-speed profiles that survived our quality controls. The plot shows profiles from 10 different months of SHEBA, November 1997 to September 1998. The wind-speed axis is relative rather than absolute; adjacent profiles are offset by 4 m s^{-1}. The number under each profile gives the wind speed at a height of 10 m. The solid lines are the fits based on least-squares linear regression with (4.1) as our model.

surface in late August. Perovich, Tucker & Ligett (2002), Sturm, Holmgren & Perovich (2002), Uttal *et al.* (2002), and Perovich et al. (2003) document these changes in the surface around the SHEBA ice camp and present many photos of surface conditions.

For the Ice Station Weddell data, we were likewise careful to exclude from our analysis any measurements that may have been disturbed by buildings or structures in the ice camp (Andreas & Claffey 1995). Our instruments at the ISW camp sampled over an undisturbed sector of 160°. The upwind surface in this sector featured snow-covered sea ice for hundreds of kilometres for the duration of our measurements.

As our fourth quality control, when we fitted the profile data according to (4.1), we computed the correlation coefficient r for the $U(z)$-*vs.*-$\ln(z)$ pairs. We kept for subsequent analysis only profiles for which $r \geqslant 0.99$. Figure 3 shows ten typical profiles from SHEBA that survived these four quality controls. The solid lines in the figure satisfy (4.1) and yielded the values for S and I that we use in our subsequent analysis. Andreas & Claffey (1995) show ten similar examples of acceptable profiles from Ice Station Weddell.

4.2. *Further checks for near-neutral stratification*

The previous constraints reduced our original (approximately) 8000 h of recorded SHEBA data to 641 hourly averaged profiles. For each of these profiles, we computed a median value of the Obukhov length, L_{med}, using $u_{*,med}$ and $\overline{w\theta}_{med}$ in (3.1), where $u_{*,med}$ and $\overline{w\theta}_{med}$ are the median values of $u_*(z)$ and the kinematic heat flux measured by the five tower sonics during the hour (Grachev *et al.* 2005). We then computed $10/L_{med}$, where 10 m is the nominal mid-level of our tower instruments. To further ensure that the profiles we retained reflected near-neutral stratification, we kept only

profiles that satisfied $-0.1 \leqslant 10/L_{med} \leqslant 0.1$. This range is the typical definition of near-neutral stratification. This screening further reduced our acceptable SHEBA profiles to 526.

Andreas & Claffey's (1995) original test for near-neutral stratification in the ISW data set was with a bulk Richardson number,

$$Ri_B = \frac{Rg}{T_s + 273.15}\left[\frac{T_s - (T_5 + \gamma R)}{U_5^2}\right]. \tag{4.4}$$

Here, R is the reference height of our sonic anemometer, 4.65 m; T_5 is the air temperature measured on the 5 m tower near the sonic; U_5 is the wind speed measured by another propeller-vane near the sonic; T_s is the snow surface temperature (°C), measured radiometrically (Andreas, Jordan & Makshtas 2004*b*); and $\gamma = g/c_p$ converts T_5 to potential temperature, where c_p is the specific heat of air at constant pressure. In the 197 one-hour profiles that survived Andreas & Claffey's screening, $|Ri_B|$ was never larger than 0.03 and was less than 0.01 for 75 % of these profiles. Thus, the ISW screening also identified profiles collected in near-neutral stratification.

4.3. *Surface value of u_**

Although we measured τ on Ice Station Weddell at only one height, all the SHEBA profiles that we retained included measurements of the local u_* at five heights. We could therefore compute u_{*0}, representative of the surface stress, by least-squares linear regression. That is, we modelled the u_* profile as

$$u_*(z) = az + b. \tag{4.5}$$

The intercept b is obviously u_{*0}.

For a strictly defined atmospheric surface layer, a in (4.5) would be zero; and $b = u_{*0}$ would equal $u_{*,med}$. Figure 4 shows the relationship between u_{*0} and $u_{*,med}$ for our data. Sometimes the $u_*(z)$ values increase with height; sometimes they decrease. Usually, in the profiles that survived our screening, u_{*0} is within 10 % of u_{*med}. We take this agreement as further evidence that our screening has produced a quality data set.

Nevertheless, to focus even more strictly on conditions for which surface-layer similarity should hold, we henceforth eliminate SHEBA profiles that yield u_{*0} values outside the interval $0.90 \leqslant u_{*0}/u_{*,med} \leqslant 1.10$. This criterion eliminated another 73 profile, finally leaving us 453.

An essential point here, though, is that even these 73 excluded SHEBA profiles met all our previous criteria. In particular, even though profiles in this newly excluded subset did not come from a constant-stress layer, they still displayed logarithmic behaviour that was as true as in the profiles that we retained. In other words, the logarithmic wind-speed profile is quite robust and can exist even without a constant-stress layer.

Frenzen & Vogel (1995*a*) faced the situation that we faced with our ISW data set. They measured τ at only one height, 2.5 m. In a desire to obtain u_{*0} for a theoretically correct evaluation of the von Kármán constant, they calculated u_* as $(\tau/\rho)^{1/2}$ but, to obtain u_{*0}, increased this value by 0.5 %, in line with the suggestion by Telford & Businger (1986). In his reply to Telford & Businger's comment, Högström (1986) likewise argued that $(\tau/\rho)^{1/2}$ measured at height z in the atmospheric surface layer should be increased to obtain an estimate of u_{*0}. However, at least over Arctic sea ice, where our instruments were well above the roughness sublayer (e.g. Frenzen & Vogel

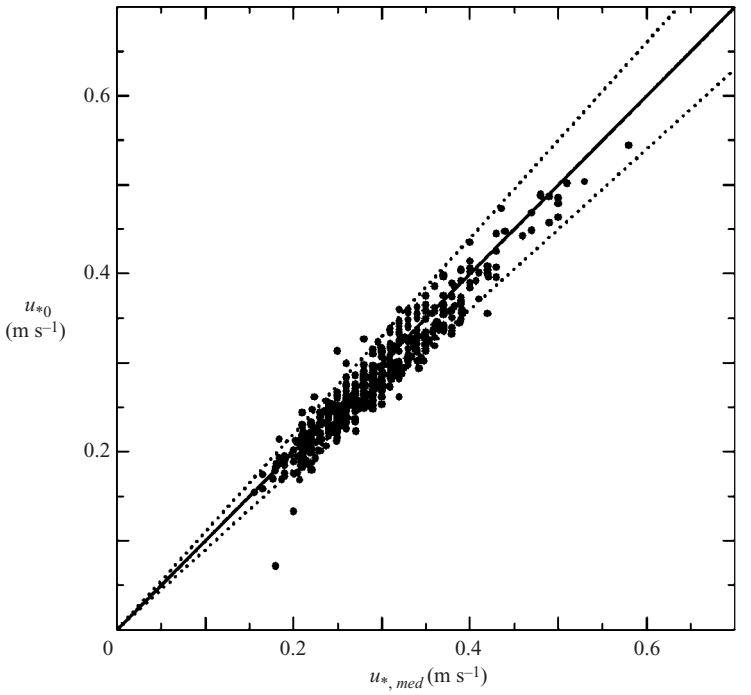

FIGURE 4. The surface value of the friction velocity, u_{*0}, from SHEBA, obtained from (4.5). The $u_{*,med}$ value is simply the median value of the five $u_*(z)$ measurements during the hour. The solid line is 1:1; the dotted lines delimit cases for which $0.90 \leqslant u_{*0}/u_{*,med} \leqslant 1.10$.

1995*b*), our data do not support this practice (i.e. figure 4). The $[\tau(z)/\rho]^{1/2} \equiv u_*(z)$ values increase with height as often as they decrease. Consequently, we use our ISW measurements of $(\tau/\rho)^{1/2}$ as if they were u_{*0} and henceforth always denote them as u_{*0}. We have reliable measurements of u_{*0} on ISW that coincide with 178 of the 197 logarithmic profiles that survived our screening.

Figure 5 shows these 178 z_0–u_{*0} pairs that survived our ISW screening and the 453 surviving pairs from SHEBA. Because we required winds of at least 4 m s^{-1}, the u_{*0} values are all larger than 0.15 m s^{-1}. The z_0 values, which we obtained from (4.3), span a range of over three orders of magnitude. Such a range of roughness lengths, however, is not atypical of snow-covered or sea-ice surfaces (e.g. Inoue 1989; Guest & Davidson 1991; Andreas & Claffey 1995; Andreas *et al.* 2005*a*). The z_0 values from ISW, which we collected during a 35 day period over snow-covered ice, have a narrower spread than the SHEBA values, which represent the full SHEBA deployment year.

In figure 5, the average u_{*0} for the SHEBA data is 0.29 m s^{-1}; for the ISW data, 0.32 m s^{-1}. For z_0, the average in the SHEBA set is 0.4–1 mm, depending on whether we compute arithmetic or geometric averages; for the ISW set, the z_0 values average 1 mm. For a typical value of the kinematic viscosity for our conditions, 1.2×10^{-5} m^2 s^{-1}, these averages yield a roughness Reynolds number that is 10–27, well into the aerodynamically rough regime, on average. The two lines in figure 5 show the aerodynamically smooth limit, where $Re_* = 0.135$ [see (2.8)], and the aerodynamically rough limit, where $Re_* = 2.5$, and thus demonstrate that most of our data come from aerodynamically rough flow.

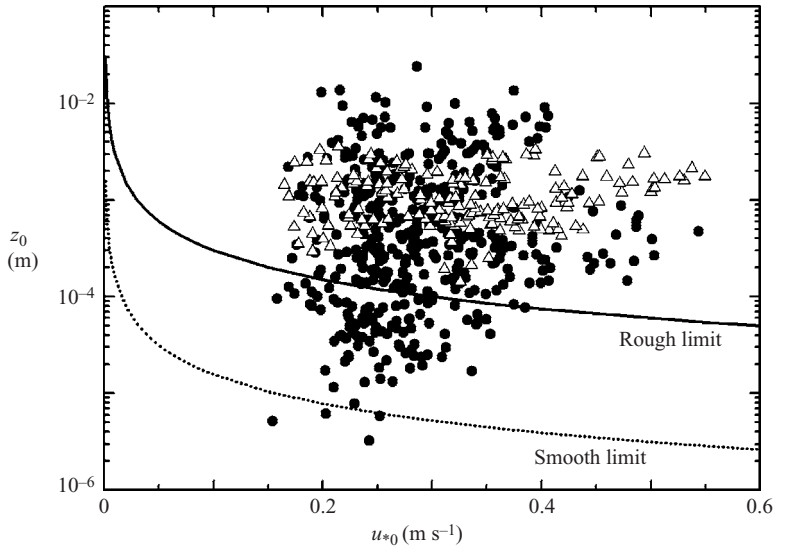

FIGURE 5. ●, The 453 z_0 and u_{*0} values from SHEBA and △, the 178 values from Ice Station Weddell that survived our screening. The lines show the aerodynamically smooth (i.e. where $Re_* = 0.135$) and aerodynamically rough (i.e. where $Re_* = 2.5$) limits, with ν assumed to be 1.2×10^{-5} m^2 s^{-1}.

5. The von Kármán constant

5.1. *Stratification correction*

In Monin–Obukhov similarity theory, which systematizes our understanding of the atmospheric surface layer, the vertical wind speed gradient in (2.2) is written in general as

$$\frac{\partial U}{\partial z} = \frac{u_{*0}}{kz}\phi_m(z/L). \tag{5.1}$$

The definition of k requires that the stratification correction ϕ_m be one for neutral stability ($z/L = 0$).

After we evaluated k for the cases that survived our screening, we checked for a residual stratification dependence. That is, we asked whether ϕ_m was one for all cases. Figures 6 and 7 show the resulting SHEBA and ISW k values plotted against the stratification parameter $\langle z\rangle/L$. Here, $\langle z\rangle$ is the geometric mean of the profile heights, and L is the measured Obukhov length. Figure 7 shows fewer ISW points than figure 5 – 100 points compared to 178 – because we did not have measurements of L for all of the ISW profiles.

Figures 6 and 7 demonstrate that our screening selected conditions very near neutral stability, but values of the von Kármán constant still depend on stratification. In these figures, we denote the von Kármán constant as k_{uc} because the values are uncorrected for residual stratification effects. In light of (5.1), figures 6 and 7, in effect, show

$$k_{uc} = \frac{k}{\phi_m(z/L)}, \tag{5.2}$$

where k is the true von Kármán constant. The lines in the two figures represent this relation with $k = 0.40$, with (Paulson 1970)

$$\phi_m(z/L) = [1 - 16(z/L)]^{-1/4} \quad \text{for } z/L < 0, \tag{5.3a}$$

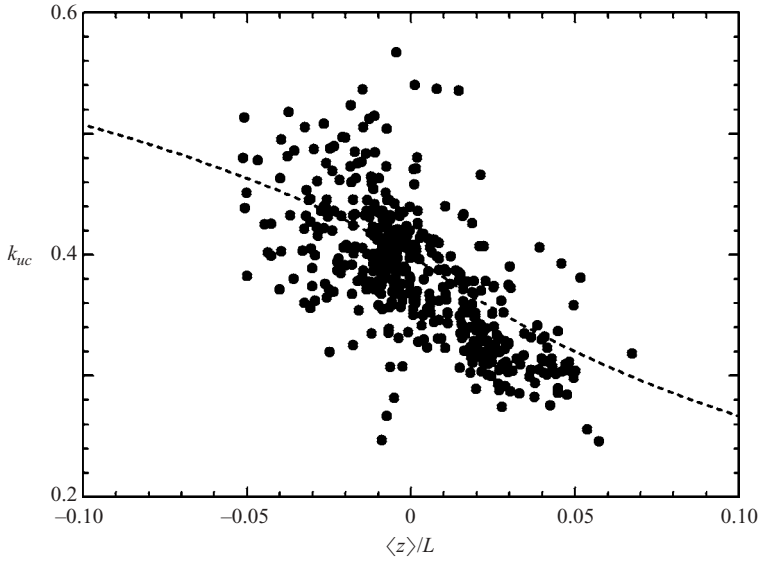

FIGURE 6. The uncorrected SHEBA k values as a function of the stratification, where $\langle z \rangle$ is the geometric mean of the five measurement heights and L is the median value of the five measured Obukhov lengths. The line is (5.2).

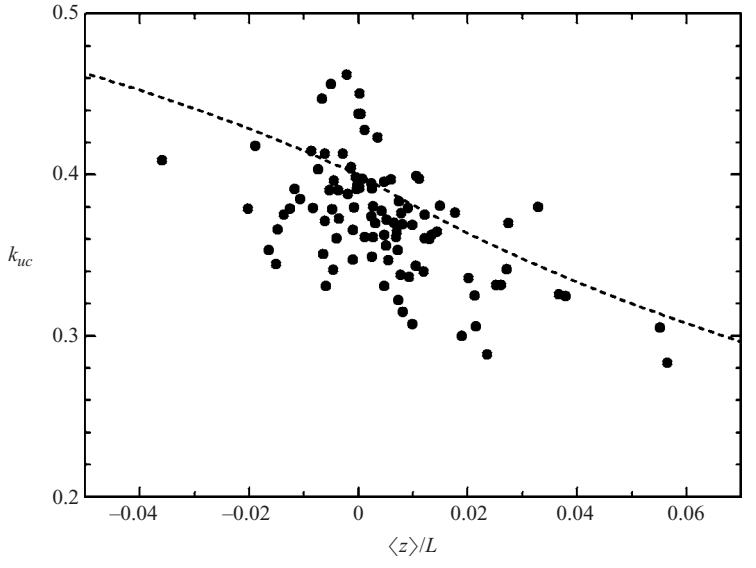

FIGURE 7. As in figure 6, except these are the Ice Station Weddell values. Quantity $\langle z \rangle$ is the geometric mean of the four profile heights, and L is the measured Obukhov length.

and with (Dyer 1974)

$$\phi_m(z/L) = 1 + 5(z/L) \quad \text{for } z/L > 0, \tag{5.3b}$$

Using (5.2) and (5.3), we can obtain stability-corrected values of the von Kármán constant from the data plotted in figure 6 and 7; that is,

$$k_{sc} = k_{uc}\phi_m(\langle z \rangle / L). \tag{5.4}$$

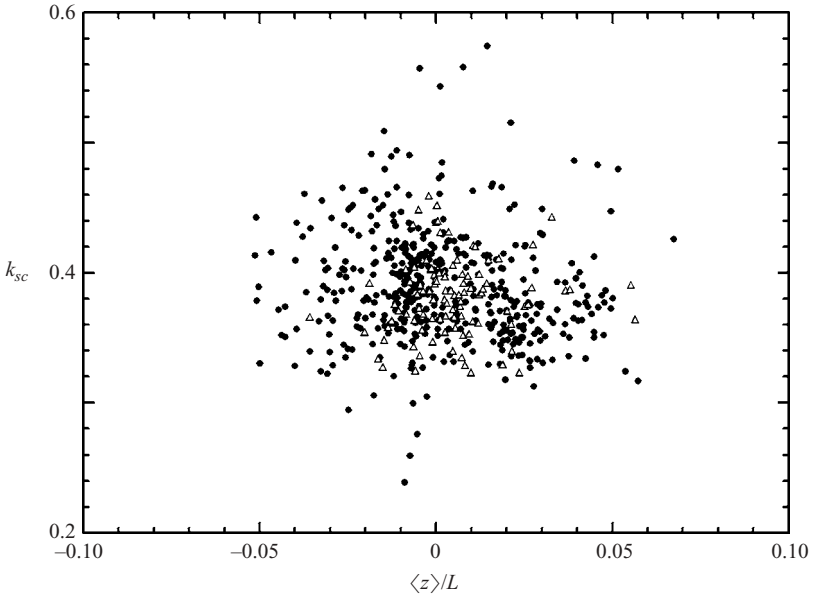

FIGURE 8. Stability-corrected values of the von Kármán constant ●, from SHEBA and △, from Ice Station Weddell.

Figure 8 demonstrates that this correction removed the stratification effects in our measurements of the von Kármán constant; it thus represents our final data set. From over 8000 h of operation at SHEBA, we gleaned 453 h of data that satisfied our requirements. Likewise, we reduced over 2200 h of data from Ice Station Weddell to the 100 best hours for our analysis.

5.2. *k as a function of Re_**

To test the idea that the von Kármán constant depends on the roughness Reynolds number, we plot our stability-corrected k values versus Re_* in figure 9. (These values are k_{sc} from figure 8, but we henceforth drop the subscript *sc* in our plots and text because we refer exclusively to these values now.) This figure seems to suggest that k is a function of the roughness Reynolds number in the atmospheric surface layer. For Re_* nominally above 6, the k values decrease markedly with increasing Re_*. For Re_* less than about 6, on the other hand, the k values bend over and tend toward the constant value 0.421 reported by McKeon *et al.* (2004).

Figure 9 also shows our least-squares fit (denoted 'Best fit') to both the SHEBA and ISW data for which $Re_* \geqslant 6$. That line is

$$k = -0.0148 \ln(Re_*) + 0.427, \tag{5.5}$$

and the correlation coefficient of these $k - \ln(Re_*)$ pairs is -0.429.

The summary results from Oncley *et al.* (1996) for $6 \leqslant Re_* \leqslant 1000$ depicted in figure 9 agree well with our best fit. The Frenzen & Vogel (1995*a*) line in the figure tends to be above our results and to depend more weakly on Re_*.

5.3. *Uncertainty analysis*

We should now backtrack a bit to consider whether the variability in k that figure 9 depicts is real or is a consequence of measurement uncertainty. We base this

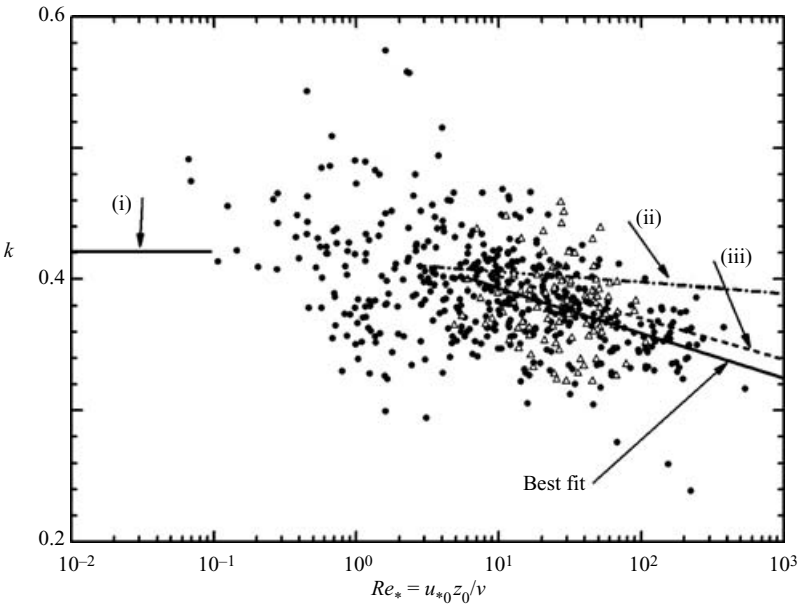

FIGURE 9. The stability-corrected ●, SHEBA and △, Ice Station Weddell values of the von Kármán constant are plotted against measured values of the roughness Reynolds number. The plot also shows tendencies and roughness Reynolds number ranges for the k values that (i) McKeon *et al.* (2004), (ii) Frenzen & Vogel (1995*a*) and (iii) Oncley *et al.* (1996) deduce. The 'Best fit' line is (5.5).

uncertainty analysis on the SHEBA data; the ISW measurements would yield similar results.

The SHEBA values of k and z_0 that we use to construct figure 9 come from our profile analysis from (4.1) to (4.3). We assign the following uncertainties to our five profile heights: ± 0.2 m at z_1, z_2 and z_3 (which were at 2.2, 3.2 and 5.1 m on average), ± 0.3 m at z_4 (8.9 m on average), and ± 0.5 m at z_5 (typically 14 or 18 m). These uncertainties reflect the fact that the base of our tower accumulated snow; we were, thus, unable to measure heights directly to a pristine snow surface. Although we list average heights above, for our calculations, we used actual height estimates at each hour. We obtained these by interpolating between occasional direct height measurements using frequent measurements of snow depth (Persson *et al.* 2002).

Based on our experience with ATI sonic anemometers, we estimate that these yield the wind speed for an hour of averaging with an uncertainty of $\pm 0.03\,\mathrm{m\,s^{-1}}$. We arrive at this figure from measurements of the standard deviation of the wind speed, σ_u, which is typically 10 % of the mean wind speed (Panofsky & Dutton 1984, p. 166ff.; Arya 1988, p. 153ff.). For example, Fairall *et al.* (1996, table 1) give a value of $0.3\,\mathrm{m\,s^{-1}}$ as the typical standard deviation based on 50 min averages for wind speeds in the range we encountered. An estimate of the error in the mean wind speed is, thus, $(0.3\,\mathrm{m\,s^{-1}})/\sqrt{N}$, where N is the number of independent samples used to construct the average. Since wind speed has a decorrelation time that is nominally 10 s (e.g. Treviño & Andreas 2000), N for the Fairall *et al.* observations is about 300, and $\sigma_u/\sqrt{N} \approx 0.02\,\mathrm{m\,s^{-1}}$. Since we average for an hour, our uncertainty estimate for the mean wind speed of $\pm 0.03\,\mathrm{m\,s^{-1}}$ is conservative.

As a conservative estimate for the uncertainty in the slope S that we derive from our profile analysis, consider

$$S \simeq \frac{(U_5 \pm 0.03) - (U_1 \pm 0.03)}{\ln[(z_5 \pm 0.5)/(z_1 \pm 0.2)]}. \tag{5.6}$$

Since $U_5 - U_1$ is typically $1.5\,\mathrm{m\,s^{-1}}$ (see figure 3), (5.6) implies

$$S \simeq \frac{(U_5 - U_1) \pm 4\%}{\ln(z_5/z_1) \pm 7\%}, \tag{5.7}$$

where, to be conservative, we used $z_5 = 14\,\mathrm{m}$ rather than 18 m. Equation (5.7) implies that S has an uncertainty of about $\pm 11\,\%$.

Individual measurements of u_* can be uncertain by $\pm 10\,\%$ (e.g. Finkelstein & Sims 2001). Since we use five independent measurements of u_* to determine the median of u_*, $u_{*,med}$, a typical uncertainty for $u_{*,med}$ is $\pm 10\,\%/\sqrt{5} = \pm 4.5\,\%$. Further, since we required that u_{*0} be within 10 % of $u_{*,med}$ (see figure 4), we take $\pm 4.5\,\%(1 \pm 10\%) = 5\%$ as the uncertainty in $u_{*,0}$.

The function ϕ_m that we use in (5.4) to remove stratification effects is also uncertain. In near-neutral but unstable stratification, the basic form of (5.3*a*) is well accepted; but the multiplicative constant 16 has been reported to range, typically, from 14 to 20 (e.g. Sorbjan 1989, p. 74; Högström 1996). Since $\langle z \rangle / L$ is hardly ever smaller than -0.05 in our application (i.e. figures 6–8), this range of choices suggests a maximum uncertainty for ϕ_m in unstable stratification of 2.6 %.

Likewise, in near-neutral but stable stratification, (5.3*b*) is an acceptable form for the stratification correction; but the multiplicative constant 5 is typically reported to range from 4 to 6 (e.g. Sorbjan 1989, p. 76; Högström 1996). Again, since $\langle z \rangle / L$ is rarely above 0.05 in our application, our choice of ϕ_m in stable stratification has a maximum uncertainty of 4 %.

Because most of our data cluster between $\langle z \rangle / L$ values of -0.02 and 0.02, we will take $\pm 2\,\%$ as the typical uncertainty in ϕ_m.

From (4.2) and (5.2), these considerations suggest

$$k = \frac{u_{*0} \pm 5\%}{(S \pm 11\%)(\phi_m \pm 2\%)}. \tag{5.8}$$

That is, individual measurements of the stability-corrected k values in figure 9 may be uncertain by $\pm 18\,\%$. The average k value of all points shown in figure 9 is 0.387; consequently, we should realistically expect our measurements of k to be scattered between 0.317 and 0.457. In fact, only 39 of the 553 k values (7 %) in figure 9 are outside this range. The variability in k in figure 9, therefore, may result largely from measurement uncertainty despite the trend with Re_*.

We estimate the uncertainty in the Re_* values in figure 9 along these same lines and find that individual estimates of Re_* may range from 45 % to 240 % of the true value. Essentially, Re_* is uncertain by a factor of two; uncertainty in z_0 causes most of this uncertainty. Nevertheless, figure 9, which shows Re_* ranging from about 0.1 to 500, realistically depicts that we experienced a wide range of roughness conditions during our measurements.

5.4. *Evidence of a constant-stress layer*

Earlier, we fitted the local friction velocity profile $u_*(z)$ with a linear function of z. Since our tower levels were roughly logarithmically spaced, it is also reasonable to evaluate the divergence in $u_*(z)$ as $\partial u_* / \partial \ln(z)$. Further, we define a non-dimensional

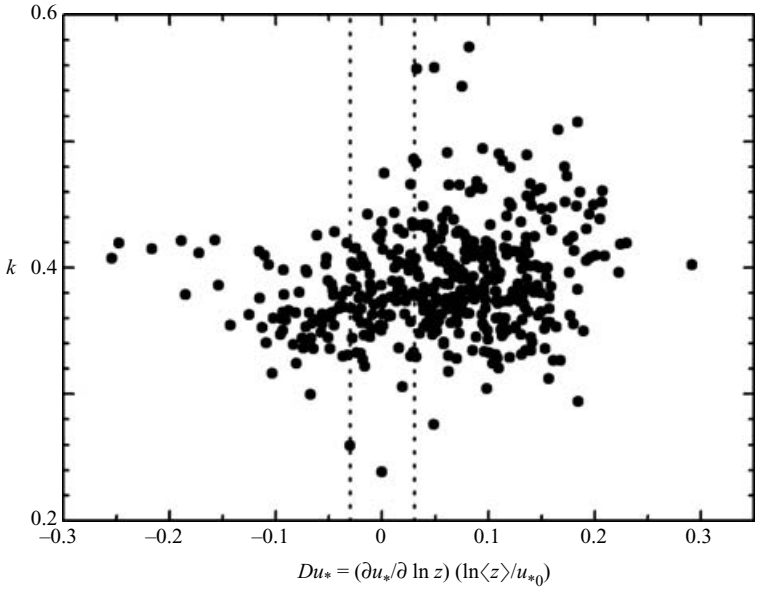

FIGURE 10. Our stability-corrected values of the von Kármán constant evaluated from the SHEBA data are plotted against the non-dimensional divergence in u_* with height. The dashed lines are at $Du_* = -0.03$ and $Du_* = 0.03$ and delimit values collected in a constant-stress layer.

flux divergence as

$$Du_* \equiv \frac{\partial u_*}{\partial \ln(z)} \frac{\ln\langle z\rangle}{u_{*0}}. \tag{5.9}$$

Here, we use least-squares linear regression to compute $\partial u_*/\partial \ln(z)$, and $\ln\langle z\rangle$ is the natural log of the geometric mean height, which is equivalent to the average of the logs of the five tower levels. As always, we evaluate (5.9) only when all five values of $u_*(z)$ are available.

Figure 10 shows values of the stability-corrected SHEBA k values plotted against Du_*. In a constant-stress layer, Du_* would be zero. As figure 4, figure 10 demonstrates that, even though our SHEBA wind-speed profiles were collected in near-neutral stratification and exhibited logarithmic behaviour, they did not necessarily come from a constant-stress layer. Also as figure 4, figure 10 shows that $u_*(z)$ can both increase and decrease with height, contrary to the assumption usually used to correct k values derived from a single measurement of τ.

In figure 10, the cases with large positive Du_* yield the largest k values. We can provisionally eliminate these largest k values from our analysis by arbitrarily assuming that profiles for which Du_* is in [−0.03, 0.03] reflect a constant-stress layer; these should be our best data. The dashed lines in figure 10 delimit this region, which contains 83 points. Still, even with this focus on a constant-stress layer, the k values in figure 10 do not show any obvious tendencies with Du_*.

Table 1 summarizes the statistics of our measured k values for various sorting categories, including the Du_* categories. We can use the statistic

$$\Sigma = \frac{\overline{x}_1 - \overline{x}_2}{\left(\sigma_1^2/N_2 + \sigma_2^2/N_1\right)^{1/2}} \tag{5.10}$$

Data set	Number	Average	Standard deviation	2SDM
SHEBA				
All	453	0.389	0.042	0.004
For Du_* in [−0.03, 0.03]	83	0.383	0.038	0.008
For Du_* outside [−0.03, 0.03]	370	0.390	0.043	0.004
Winter	272	0.396	0.042	0.005
Summer	181	0.379	0.041	0.006
Ice Station Weddell	100	0.381	0.030	0.006
Combined SHEBA & ISW	553	0.387	0.041	0.003

TABLE 1. Summary of average von Kármán constants. '2SDM' is twice the standard deviation of the mean, which approximately defines the 95 % confidence interval for the 'Average'.

to test the hypothesis that the averages in any two categories in table 1 are different. Here, $\overline{x}$ is the average k value for a category in the table, σ is the corresponding sample standard deviation, and N is the number of samples in the category. This Σ statistic is normally distributed with mean zero and standard deviation 1 when N_1 and N_2 are large. For all categories in table 1, the samples sizes are large enough to satisfy this condition.

When $\overline{x}_1$ and $\overline{x}_2$ in (5.10) are the average k values when Du_* is within and outside the interval [−0.03, 0.03], respectively, $\Sigma = -1.38$. Thus, we would accept the hypothesis that k is smaller when Du_* is in [−0.03, 0.03] than when it is outside this interval only at the 8 % significance level. Because 8 % is a fairly large significance level for a one-sided test, our data suggest that the von Kármán constant has the same value whether the stress is constant with height or changes by roughly ±20 % over a layer 12–16 m thick.

6. Artificial correlation

6.1. *In the k-Re_* measurements*

A troubling feature of our analysis is that evaluating k requires u_{*0} and the slope S of the logarithmic profile, while evaluating Re_* also requires u_{*0} and z_0; and z_0 derives from S through (4.3). As a result, because of the shared variables, k and Re_* may have built-in correlation that does not reflect any physics (e.g. Hicks 1978*a*, *b*; Kenney 1982; Firebaugh & Gibbs 1985; Kronmal 1993; Andreas & Hicks 2002). In the Appendix, we use techniques suggested by Hicks (1978*b*) and Andreas (2002) to quantify this artificial correlation.

That analysis suggests that, because of the shared variables, the SHEBA and ISW k–$\ln(Re_*)$ pairs for which $Re_* \geqslant 6$ have a built-in correlation with a correlation coefficient of $r_a = -0.396$ (subscript a for artificial). Compare this with the experimental correlation coefficient, $r_d = -0.429$ (subscript d for data), for these same data. Moreover, the analysis in the Appendix lets us compute the least-squares regression line for the artificial correlation of these data as

$$k = -0.0220 \ln (Re_*) + 0.451. \tag{6.1}$$

Compare this with (5.5).

Figure 11 reproduces the plot from figure 9, but here we identify the SHEBA points for which Du_* is in [−0.03, 0.03], presumably our most reliable data. These best points, however, do not exhibit behaviour that differs significantly from the

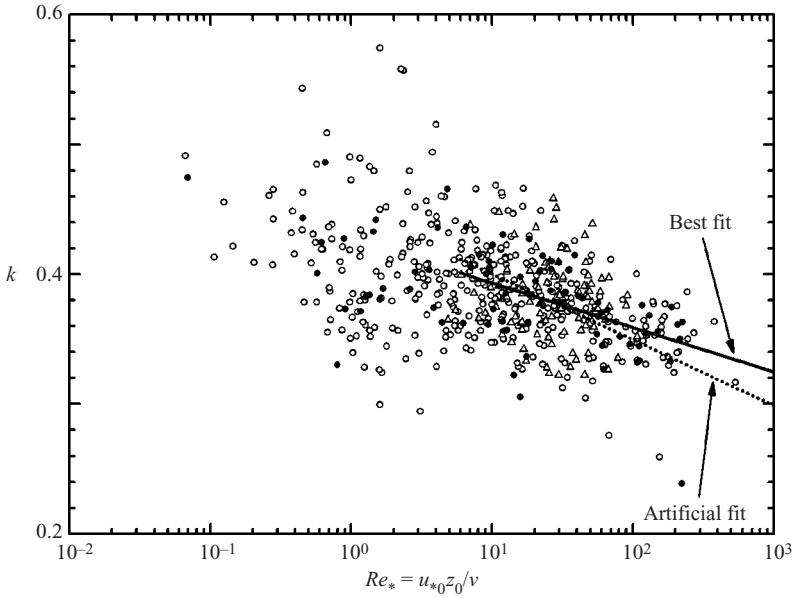

FIGURE 11. The stability-corrected von Kármán constants are again plotted against the measured roughness Reynolds number. The plot identifies the SHEBA points ●, that were collected in a constant-flux layer, where $-0.03 \leqslant Du_* \leqslant 0.03$, and ○, outside, as identified in figure 10. △, Ice Station Weddell. The plot again shows our 'Best fit' line, (5.5), and the line suggested by the artificial correlation required by the shared variables in k and Re_*, (6.1) ('Artificial fit').

entire data set in general. In particular, for $Re_* \geqslant 6$, these best points still scatter fairly uniformly about the 'best fit' line that we determined using the whole data set.

In figure 11, we also include the correlation line (6.1) (denoted 'Artificial fit'). This line is similar to our best-fit line and also reasonably captures the trend in k with Re_* for $Re_* \geqslant 6$.

We can calculate a confidence interval for the correlation coefficient r_a to help us decide whether the artificial correlation is largely responsible for the decrease in k with Re_* that we see in figure 11. Bendat & Piersol (1971, p. 126ff.) explain that the statistic

$$\omega(r) = \tfrac{1}{2} \ln\left(\frac{1+r}{1-r}\right), \tag{6.2}$$

where r is the correlation coefficient, has a normal distribution with mean $\overline{\omega} = \omega(r_a)$ and variance

$$\sigma_\omega^2 = \frac{1}{N-3}, \tag{6.3}$$

where $N(= 383)$ is the number of k–Re_* data pairs for which $Re_* \geqslant 6$ in our data set.

Using this information, we can define a confidence interval for ω from the probability statement

$$Pr\left\{ -z_{\varepsilon/2} \leqslant \frac{\omega - \overline{\omega}}{\sigma_\omega} \leqslant z_{\varepsilon/2} \right\} = 1 - \varepsilon. \tag{6.4}$$

Here, $z_{\varepsilon/2}$ is the $100(1-\varepsilon/2)$ percentage point of a normal distribution. If $\varepsilon = 0.05$, $z_{\varepsilon/2} = 1.96$; and (6.4) defines a 95 % confidence interval.

On using (6.2) to express (6.4) in terms of r, rearranging, obtaining $\overline{\omega} = -0.419$ for $r_a = -0.396$ from (6.2) and $\sigma_\omega = 0.0513$ from (6.3), we finally obtain a probability statement for the correlation coefficient;

$$Pr\{-0.477 \leqslant r \leqslant -0.308\} = 95\%. \tag{6.5}$$

That is, $[-0.477, -0.308]$ is a 95 % confidence interval for the artificial correlation coefficient. Since the actual correlation coefficient for the k–$\ln(Re_*)$ data for $Re_* \geqslant 6$, $r_d = -0.429$, is well within this interval, we cannot attribute any real dependence on Re_* to the k values in figure 11. The trend we find in k for $Re_* \geqslant 6$ results strictly from artificial correlation. We suspect that artificial correlation also influenced the conclusion in Frenzen & Vogel (1995*a*) and Oncley *et al.* (1996) that k depends on Re_*.

6.2. *Bulk flux estimate of* Re_*

The artificial correlation arises because we use the same measurements to evaluate both k and Re_*. If we could make an independent estimate of Re_*, we would find a more reliable answer to our question of whether k depends on Re_*. We thus estimate u_{*0} and z_0 – and therefore Re_* – from a bulk flux algorithm.

The bulk flux method (e.g. Fairall *et al.* 1996, 2003) derives from Monin–Obukhov similarity theory. The surface stress and the fluxes of sensible (H_s) and latent (H_L) heat are expressed as

$$\tau \equiv \rho u_{*0}^2 = \rho C_{DR} U_R^2, \tag{6.6a}$$

$$H_s \equiv \rho c_p \overline{w\theta} = \rho c_p C_{HR} U_R (\Theta_s - \Theta_R), \tag{6.6b}$$

$$H_L \equiv \rho L_v \overline{wq} = \rho L_v C_{ER} U_R (Q_s - Q_R). \tag{6.6c}$$

Here, c_p is the specific heat of air at constant pressure; L_v, the latent heat of sublimation (over ice and snow, remember); $\overline{wq}$, the flux of specific humidity, where q is the turbulent fluctuation in specific humidity; U_R, Θ_R and Q_R, the mean wind speed, potential temperature and specific humidity at reference height R; and Θ_s and Q_s, the temperature and humidity at the surface.

The key to the bulk flux method is specifying the transfer coefficients for momentum (C_{DR}, also called the drag coefficient) and for sensible (C_{HR}) and latent (C_{ER}) heat. We report our parameterization for these over sea ice elsewhere (Jordan, Andreas & Makshtas 1999; Andreas 1987, 2002; Andreas *et al.* 2004*a*, *b*, 2005*a*, *b*). Realize, too, that, although we primarily want to predict u_{*0} and z_0, we must carry the H_s and H_L equations in our bulk flux algorithm because the Obukhov length L (required to compute C_{DR}, C_{HR} and C_{ER}) depends on τ, H_s and H_L (see (3.1)). Thus, we must solve the bulk flux equations iteratively.

Figure 12 shows the results of our calculations with this bulk flux algorithm. Here, we have used our algorithm to make a 'bulk' estimate of the roughness Reynolds number, $Re_{*,Bulk}$, for each set of conditions that provided a k value. In other words, in $Re_{*,Bulk}$, the u_{*0} and z_0 values now come strictly from our algorithm. The figure also shows the least-squares fit of the k–$\ln(Re_{*,Bulk})$ pairs for the Ice Station Weddell set, for the SHEBA set, and for the combined set.

The correlation coefficient for the ISW k–$\ln(Re_{*,Bulk})$ data in figure 12 is –0.209. Using the same procedure as in the last section, we compute the 95 % confidence interval on this correlation coefficient to be [–0.390, –0.012]. That is, the ISW line in figure 12 is statistically different from horizontal (i.e. the correlation coefficient would equal zero) at the 5 % significance level – but just barely. However, the fitting lines for the SHEBA and combined sets in figure 12 have correlation coefficients of –0.003 and

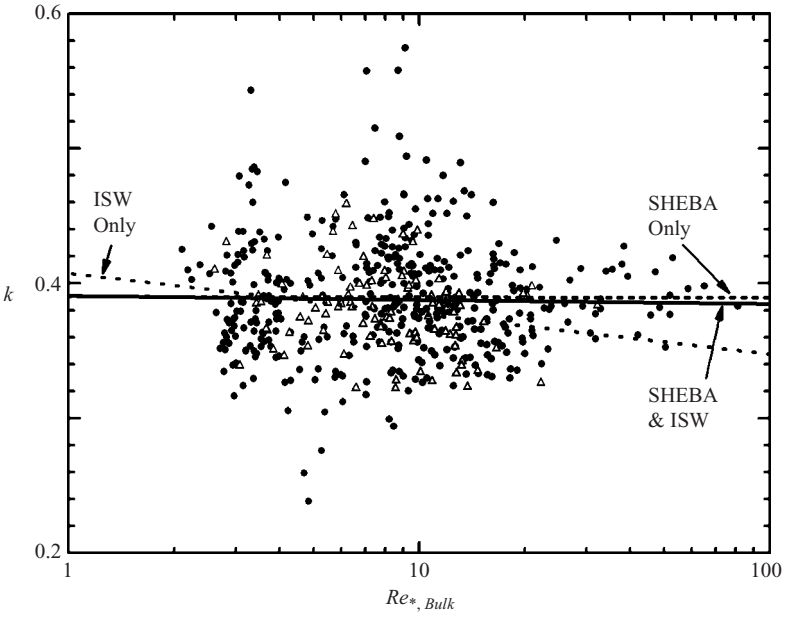

FIGURE 12. The stability-corrected von Kármán constants are plotted against corresponding estimates of the roughness Reynolds number from our bulk flux algorithm. The lines show the least-squares fits of △, the Ice Station Weddell data; ●, the SHEBA data, and the combined set.

–0.021, respectively, and these mean that k has no statistically significant correlation with our bulk estimate of the roughness Reynolds number in these larger data sets.

In summary, this analysis reiterates our conclusion in the last section: our measurements of the von Kármán constant exhibit no dependence on the roughness Reynolds number for $2 \leqslant Re_{*,Bulk} \leqslant 100$.

7. Discussion

7.1. *The inconstancy of stress with height*

Although all 453 of the SHEBA wind speed profiles that we used in our final analysis show a logarithmic dependence on height, as depicted in figure 3, few of these also exhibit a corresponding layer of constant stress. With u_* as a surrogate for this stress, we establish this fact with figures 4 and 10. We here speculate on the reasons for this variability in stress with height.

In the atmospheric surface layer, the equation for the mean longitudinal velocity component, $U(z)$, derives from the Navier–Stokes equation under the assumptions of a large Reynolds number and horizontal homogeneity (e.g. Busch 1973; Businger 1982);

$$\frac{\partial U(z)}{\partial t} = -\frac{\partial \overline{uw}}{\partial z} + f_C[V(z) - V_g]. \tag{7.1}$$

Here, f_C is the Coriolis parameter, $V(z)$ is the mean transverse velocity component (zero in our coordinate system), and V_g is the transverse component of the geostrophic wind. On scaling (7.1) with u_{*0} and z_0, we obtain (cf. Tennekes 1982)

$$\frac{\partial(U/u_{*0})}{\partial(u_{*0}\,t/z_0)} = -\frac{\partial\left(\overline{uw}/u_{*0}^2\right)}{\partial(z/z_0)} - \frac{f_C z_0}{u_{*0}}\left(\frac{V_g}{u_{*0}}\right). \tag{7.2}$$

We recognize $u_{*0}/f_C\,z_0$ as the surface Rossby number, Ro_*, and evaluate this to have been about 2×10^6 for both SHEBA and Ice Station Weddell for typical values for u_{*0} and z_0 that we have already discussed. Further, u_{*0}/V_g is comparable to the geostrophic drag coefficient, which commonly ranges between 0.01 and 0.05 over sea ice (Overland & Davidson 1992; Overland & Colony 1994; Andreas 1998). Therefore, the right-most term in (7.2) is of order 10^{-5} and, thus, negligible. The variation in $\overline{uw}$ with height may consequently result from non-stationarity;

$$\frac{\partial U}{\partial t} \approx -\frac{\partial\overline{uw}}{\partial z}. \tag{7.3}$$

Because of figure 4, we excluded SHEBA profiles for which $u_*(z)$ varied by more than about 10 % between the top and bottom instruments on our tower. Thus, $\partial\overline{uw} \approx (\Delta u_*)^2 \approx 0.001\,\mathrm{m^2\,s^{-2}}$ for a typical SHEBA u_* value of $0.3\,\mathrm{m\,s^{-1}}$. Likewise, $\partial z \approx \Delta z$ was between 12 and 16 m. For demonstration purposes, take $\Delta z = 15\,\mathrm{m}$. Consequently, we estimate the maximum wind speed change that could have occurred during any hour of SHEBA data that we retained to be $\Delta U = \pm(0.001)\,\mathrm{m^2\,s^{-2}}/15\,\mathrm{m})(3600\,\mathrm{s}) = \pm 0.2\,\mathrm{m\,s^{-1}}$. Because this is not an unusually large change in wind speed, non-stationarity could explain the variability in stress with height. Notice, too, that this mechanism causes stress to both increase and decrease with height, as we observed (figure 10).

Another explanation for the variability in stress with height could be the shallowness of the atmospheric boundary layer. Because of the high emissivity and high albedo of a sea ice surface, the absence of sunlight during the winter, and the low sun angle when the sun is up, sea ice usually loses long-wave radiation to space (Intrieri *et al.* 2002). The resulting stable atmospheric layer over the sea ice, however, is frequently elevated. In other words, the base of the inversion layer is not always at the surface over either Arctic or Antarctic sea ice (Kahl 1990; Serreze, Kahl & Schnell 1992; Andreas, Claffey & Makshtas 2000); and between the surface and the inversion base, the atmosphere can have neutral or weakly unstable stratification. With either a surface-based or an elevated inversion, though, because of the overriding inversion layer, the atmospheric boundary layer can be quite shallow. On Ice Station Weddell, for instance, boundary-layer depths h under 100 m were not unusual (e.g. Andreas *et al.* 2000).

Caughey, Wyngaard & Kaimal (1979) and Nieuwstadt (1984) show non-dimensional stress, $-\overline{uw}/u_{*0}^2$, plotted versus non-dimensional height, z/h, from observations over land in stable stratification. Both plots suggest that $-\overline{uw}$ can decrease to roughly 70 % of its surface value over the lower 20 % of a stable boundary layer (see also Garratt 1992, p. 167ff.). For a 100 m deep atmospheric boundary layer, these observations imply that $u_*(z)$ might decrease to about 80 % of u_{*0} at the top of our 20 m tower.

Again, these estimates are in line with what we observed. However, this shallow stable boundary layer argument explains only a decrease in $u_*(z)$ with height, while figure 10 shows that $u_*(z)$ increased with height more often than it decreased.

7.2. *Effects of drifting snow*

Another possible explanation for the variation in stress with height and, indeed, for the variability in k could be the stabilization of the near-surface atmosphere caused by drifting and blowing snow. On reviewing our measurements in light of blowing

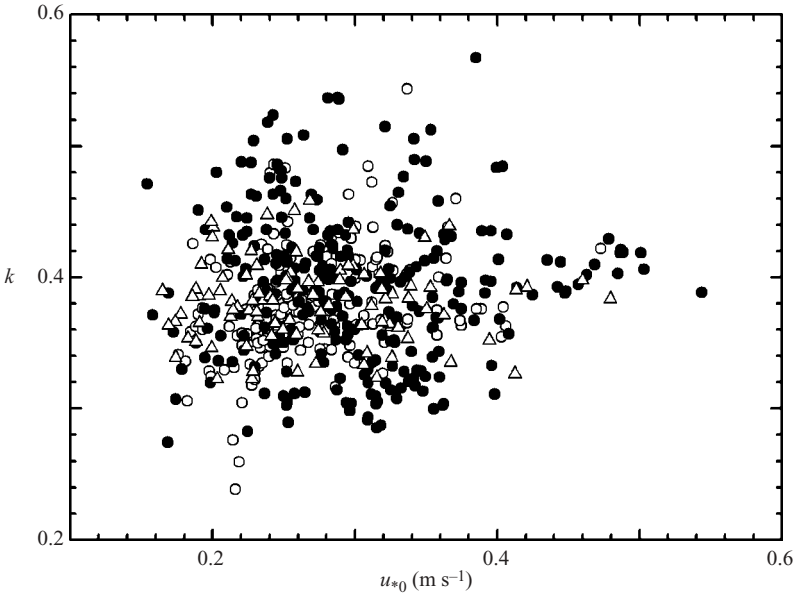

FIGURE 13. The stability-corrected von Kármán constants are plotted against the measured friction velocity. The SHEBA data are grouped according to season: ●, winter or ○, summer. All the Ice Station Weddell data (△) come from winter conditions.

snow models and analyses by Wamser & Lykossov (1995), Déry & Taylor (1996) and Bintanja (2002) and the suspended sediment model of Taylor & Dyer (1977), however, we see no reason to suspect that blowing snow affected our stress or k measurements. Our measurements of the wind-speed profile and τ were well above the region most strongly affected by blowing snow. Nevertheless, we can still query our data about possible blowing-snow effects.

Based on the behaviour of the snow surface, we divided the SHEBA year into two seasons, winter and summer. During winter, the snow was ubiquitous and dry, and the winds were occasionally strong enough to cause 'storms' of drifting and blowing snow. In summer, winds were too light or the snow was too sticky to become airborne; and for much of the summer, no snow was present on the sea ice. Winter ran from the start of the SHEBA experiment in October 1997 to 14 May 1998 and from 15 September to the end of the experiment in October 1998. Summer was the intervening period, 15 May to 14 September 1998. All of the Ice Station Weddell cases fit our definition of winter.

Figure 13 shows our SHEBA and ISW measurements of k versus u_{*0}. We have separated the SHEBA data into winter and summer measurements. The plot shows 272 SHEBA winter measurements that yield an average k value of 0.396 ± 0.005, where the uncertainty is twice the standard deviation of the mean (table 1). The plot also shows 181 SHEBA summer measurements for which k averages 0.379 ± 0.006 and 100 ISW (winter) measurements for which k averages 0.381 ± 0.006.

Over sea ice, snow begins to drift when the friction velocity reaches about 0.3 m s^{-1} (Andreas *et al.* 2004*a*, 2005*a*). Amid the clutter of points in figure 13, we do not see any obvious trends with u_{*0}; but figure 13 suffers from artificial correlation because u_{*0} appears in the calculation of k (i.e. see (4.2)). Consequently, we hesitate to infer cause and effect from figure 13.

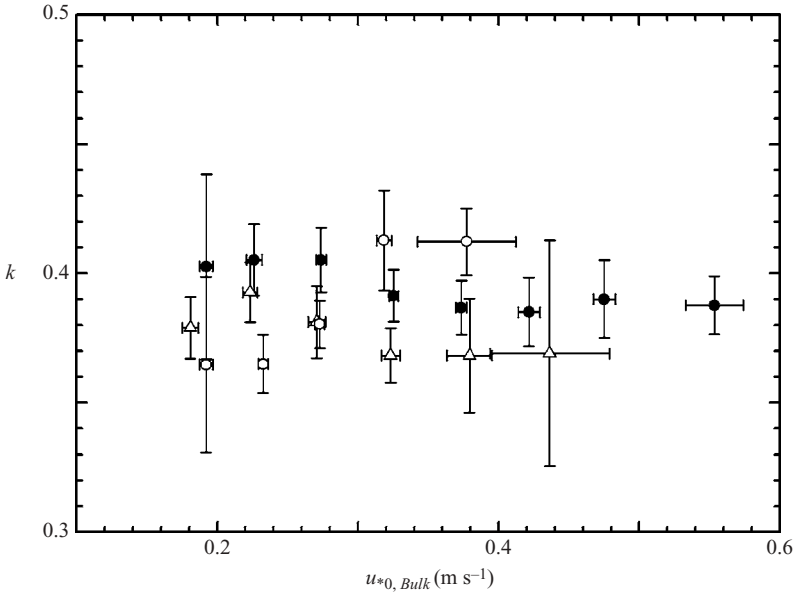

FIGURE 14. The measured von Kármán constants are averaged in bins of friction velocity computed from our bulk flux algorithm, $u_{*0,Bulk}$. Except for large $u_{*0,Bulk}$, where we have few observations, the $u_{*0,Bulk}$ bins are 5 cm s^{-1} wide. The error bars are ± 2 standard deviations in the means of k and $u_{*0,Bulk}$. ●, SHEBA winter; ○, SHEBA, summer; △, Ice Station Weddell.

Instead, we plot k as a function of the friction velocity that we obtained from our bulk flux algorithm, $u_{*0,Bulk}$. Our measurements of k have negligible artificial correlation with $u_{*0,Bulk}$. Furthermore, we bin-average the three k sets in figure 13 to obtain a better picture of tendencies with u_{*0} (figure 14).

The error bars in figure 14 mark ± 2 standard deviations in the bin means and thus show, approximately, the 95 % confidence interval for each bin-averaged value. Notice that, for the ISW and SHEBA winter sets, the bin-averaged k values do not vary significantly for $u_{*0,Bulk}$ above 0.3 m s^{-1}, where drifting and blowing snow would have been present. Thus, we again conclude that drifting snow has not affected our measurements of the von Kármán constant.

The one surprise in figure 14 is that, for the SHEBA summer set, k does seem to trend with $u_{*0,Bulk}$, although there was no blowing snow in the summer. The k values when $u_{*0,Bulk}$ is above 0.3 m s^{-1} are significantly larger than when $u_{*0,Bulk}$ is below this limit. We have no ready physical explanation for this behaviour but assume it is a statistical quirk. The SHEBA summer data fall into only five $u_{*0,Bulk}$ bins, and the bins with the smallest and largest $u_{*0,Bulk}$ contain only seven and three points, respectively.

8. Conclusions

During SHEBA, our profiling tower was instrumented and running for roughly 8000 h. Through careful screening, we retained 453 h from this set as cases that most nearly represent near-neutral stratification in an atmospheric surface layer with a nearly constant vertical stress profile. Each of these 453 profiles included the vector

wind speed $U(z)$ and eddy-covariance measurements of the stress $\tau(z)$ at each of five tower levels, nominally between 2 and 18 m.

Each of these 453 wind-speed profiles exhibited a layer, encompassing all five levels, that was logarithmic in z with a correlation coefficient of 0.99 or better. That logarithmic behaviour, however, did not require that the layer be a region of constant stress. Our $u_*(z) \equiv [\tau(z)/\rho]^{1/2}$ values both increased and decreased with height along the tower by as much as 10 %. That is, the logarithmic wind-speed profile is an experimentally robust feature of the neutrally stratified atmospheric surface layer.

On Ice Station Weddell, we ran another profiling mast that used different technology and sampled a different height range from our SHEBA tower. The ISW mast used propeller anemometers to measure $U(z)$ at four levels and operated for over 800 h in this configuration. In this set, we identified 100 hourly profiles collected in near-neutral stratification that were logarithmic in z with a correlation coefficient of at least 0.99 and for which we also measured u_{*0} and the Obukhov length L.

From the SHEBA and ISW $U(z)$ profiles and our direct measurements of u_{*0}, we made 553 independent determinations of the von Kármán constant k. Although recent literature suggests that k depends on the roughness Reynolds number Re_*, we see no reliable evidence of this behaviour in our data. When we plot k versus our measured value of Re_*, k obviously decreases with increasing Re_* for $Re_* \geqslant 6$; but we reject this evidence because the shared variables that went into calculating both k and Re_* require this trend. When we, instead, plot k versus an estimate of Re_* derived from a bulk flux algorithm – a pairing that has no artificial correlation – the k values are independent of $Re_{*,Bulk}$ for $2 \leqslant Re_{*,Bulk} \leqslant 100$. Thus, with a much larger data set, we contradict the suggestion by Frenzen & Vogel (1995*a*, *b*) and Oncley *et al.* (1996) that k depends on the roughness Reynolds number in aerodynamically rough flow.

Our combined data set does suggest that k is smaller than the canonical value of 0.40 – but not by much. The average of 553 estimates is $k = 0.387 \pm 0.003$. This value is more in line with the laboratory value for aerodynamically smooth flow of 0.38 reported by Österlund *et al.* (2000) and Nagib *et al.* (2004) than it is with the values from Zagarola & Smits (1998) and McKeon *et al.* (2004) of 0.436 and 0.421, respectively. The former two studies were in wind tunnels with zero pressure gradient; while the latter two were in the Princeton superpipe, which had a favourable pressure gradient. Our atmospheric observations featured along-wind pressure gradients that were extremely weak – at least three orders of magnitude less than the smallest gradients that Zagarola & Smits used.

Our results, thus, seem to unify the laboratory and atmospheric observations of k. When combined with the results from Österlund *et al.* (2000), Zanoun *et al.* (2003), and Nagib *et al.* (2004), our data support the conclusion that the von Kármán constant is, indeed, constant at 0.38–0.39 in all aerodynamic roughness regimes.

We thank Joost Businger and Paul Frenzen for providing historical perspective and encouragement, Keith McNaughton for pointing out relevant related work, Mark Zagarola for important insights into preparing the manuscript, and three referees for helpful comments. The US Department of the Army supported E. L A., K. J. C. and R. E. J. in this work through Project 611102T2400. The US National Science Foundation also supported this work with awards to the Army's Cold Regions Research and Engineering Laboratory (OPP-97-02025, OPP-98-14024 and OPP-00-84190), NOAA's Earth System Research Laboratory (OPP-97-01766 and OPP-00-84323), and the Naval Postgraduate School (OPP-97-01390 and OPP-00-84279).

Appendix. Artificial correlation

For the data in figure 9 for which $Re_* \geqslant 6$, our model is that k is linearly related to the logarithm of Re_*,

$$k(S, u_{*0}, \phi_m) = \alpha \ln[Re_*(u_{*0}, \nu, S, I)] + \beta. \tag{A 1}$$

We determine α and β by least-squares linear regression and quantify the goodness of this model with the correlation coefficient r, which we obtain from

$$r = \frac{\mathrm{Cov}[\ln(Re_*), k]}{\sigma_{\ln Re_*}\sigma_k}, \tag{A 2}$$

where Cov is the covariance operator, and σ_{lnRe_*} and σ_k are standard deviations of $\ln(Re_*)$ and k. Further, α and β come from

$$\alpha = \frac{\mathrm{Cov}[\ln(Re_*), k]}{\sigma^2_{\ln Re_*}} \tag{A 3}$$

and

$$\beta = \overline{k} - \alpha\,\overline{\ln(Re_*)}. \tag{A 4}$$

Here $\overline{k}$ and $\overline{\ln(Re_*)}$ are the averages of the k and $\ln(Re_*)$ values used in the fitting.

To investigate how artificial correlation affects our analysis, we evaluate r, α and β under the assumption that the fundamental quantities, u_{*0}, ν, S, I and ϕ_m, are all uncorrelated. We base this analysis on differentials (e.g. Andreas 1992) or, in Margenau & Murphy's (1956, p. 504ff.) terminology, 'residuals'.

To evaluate the standard deviations of k and $\ln(Re_*)$ and the covariance between them, start with the differential of k. Equations (4.2) and (5.4) give

$$k = \frac{u_{*0}\phi_m}{S}. \tag{A 5}$$

Therefore,

$$\mathrm{d}k = \frac{\partial k}{\partial S}\,\mathrm{d}S + \frac{\partial k}{\partial u_{*0}}\,\mathrm{d}u_{*0} + \frac{\partial k}{\partial \phi_m}\,\mathrm{d}\phi_m. \tag{A 6}$$

By using (A 5) to evaluate these partial derivatives, we obtain

$$\mathrm{d}k = -\frac{u_{*0}\,\phi_m}{S^2}\,\mathrm{d}S + \frac{\phi_m}{S}\,\mathrm{d}u_{*0} + \frac{u_{*0}}{S}\,\mathrm{d}\phi_m. \tag{A 7}$$

Similarly, from (A 1),

$$\mathrm{d}[\ln(Re_*)] = \frac{1}{Re_*}\left[\frac{\partial Re_*}{\partial u_{*0}}\,\mathrm{d}u_{*0} + \frac{\partial Re_*}{\partial \nu}\,\mathrm{d}\nu + \frac{\partial Re_*}{\partial S}\,\mathrm{d}S + \frac{\partial Re_*}{\partial I}\,\mathrm{d}I\right]; \tag{A 8}$$

while from (4.3),

$$Re_* = \frac{u_{*0}}{\nu}\exp(-I/S). \tag{A 9}$$

Equation (A 9) yields all the partial derivatives required in (A 8); (A 8) thus becomes

$$\mathrm{d}[\ln(Re_*)] = \frac{\mathrm{d}u_{*0}}{u_{*0}} - \frac{\mathrm{d}\nu}{\nu} + \frac{I\mathrm{d}S}{S^2} - \frac{\mathrm{d}I}{S}. \tag{A 10}$$

If we square (A 7), average, identify $\overline{\mathrm{d}x\mathrm{d}x} \equiv \sigma_x^2$, and invoke our assumption that all cross-terms (e.g. $\overline{\mathrm{d}S\mathrm{d}u_{*0}}$) are zero, we obtain

$$\sigma_k^2 = \frac{u_{*0}^2\phi_m^2\,\sigma_S^2}{S^4} + \frac{\phi_m^2\sigma_{u_{*0}}^2}{S^2} + \frac{u_{*0}^2\sigma_{\phi_m}^2}{S^2}. \tag{A 11}$$

Here we interpret u_{*0}, S and ϕ_m to be averages, though we have dropped the overbars. Likewise, from (A 10),

$$\sigma^2_{\ln Re_*} = \frac{\sigma^2_{u_{*0}}}{u^2_{*0}} + \frac{\sigma^2_v}{v^2} + \frac{I^2\sigma^2_S}{S^4} + \frac{\sigma^2_I}{S^2}. \tag{A 12}$$

Finally, we identify the covariance as

$$\mathrm{Cov}[\ln(Re_*), k] \equiv \overline{\mathrm{d}ln(Re_*)\,\mathrm{d}k}. \tag{A 13}$$

With (A 7) and (A 10), this becomes

$$\mathrm{Cov}[\ln(Re_*), k] = \frac{\phi_m\sigma^2_{u_{*0}}}{S\,u_{*0}} - \frac{u_{*0}\phi_m I\sigma^2_S}{S^4}. \tag{A 14}$$

Using (A 11), (A 12) and (A 14) in (A 2), (A 3) and (A 4), we can evaluate r, α and β under the assumption that none of the fundamental variables are correlated. Because the covariance between $\ln(Re_*)$ and k computed from (A 14) is non-zero in general, r and α will be non-zero; thus, k will appear correlated with $\ln(Re_*)$ simply because of the shared variables. In summary, these α, β and r values quantify the 'best' artificial fit for the k–$\ln(Re_*)$ pairs for $Re_* \geqslant 6$.

REFERENCES

Andreas, E. L 1987 A theory for the scalar roughness and the scalar transfer coefficients over snow and sea ice. *Boundary-Layer Met.* **38**, 159–184.

Andreas, E. L 1992 Uncertainty in a path-averaged measurement of the friction velocity u_*. *J. Appl. Met.* **31**, 1312–1321.

Andreas, E. L 1998 The atmospheric boundary layer over polar marine surfaces. In *Physics of Ice-Covered Seas*, vol. 2 (ed. M. Leppäranta), pp. 715–773. Helsinki University Press.

Andreas, E. L 2002 Parameterizing scalar transfer over snow and ice: a review. *J. Hydromet.* **3**, 417–432.

Andreas, E. L & Claffey, K. J. 1995 Air-ice drag coefficients in the western Weddell Sea: 1. Values deduced from profile measurements. *J. Geophys. Res.* **100**, 4821–4831.

Andreas, E. L & Hicks, B. B. 2002 Comments on 'Critical test of the validity of Monin–Obukhov similarity during convective conditions'. *J. Atmos. Sci.* **59**, 2605–2607.

Andreas, E. L & Treviño, G. 2000 Comments on 'A physical interpretation of von Kármán's constant based on asymptotic considerations – A new value'. *J. Atmos. Sci.* **57**, 1189–1192.

Andreas, E. L, Hill, R. J., Gosz, J. R., Moore, D. I., Otto, W. D. & Sarma, A. D. 1998 Statistics of surface-layer turbulence over terrain with metre-scale heterogeneity. *Boundary-Layer Met.* **86**, 379–408.

Andreas, E. L, Fairall, C. W., Guest, P. S. & Persson, P. O. G. 1999 An overview of the SHEBA atmospheric surface flux program. In *Fifth Conf. on Polar Meteorology and Oceanography*, pp. 411–416. American Meteorological Society.

Andreas, E. L, Claffey, K. J. & Makshtas, A. P. 2000 Low-level atmospheric jets and inversions over the western Weddell Sea. *Boundary-Layer Met.* **97**, 459–486.

Andreas, E. L, Jordan, R. E., Guest, P. S., Persson, P. O. G., Grachev, A. A. & Fairall, C. W. 2004*a* Roughness lengths over snow. In (CD-ROM) *18th Conf. on Hydrology*, American Meteorological Society, 8 pp. http://ams.confex.com/ams/pdfpapers/68601.pdf.

Andreas, E. L, Jordan, R. E. & Makshtas, A. P. 2004*b* Simulations of snow, ice, and near-surface atmospheric processes on Ice Station Weddell. *J. Hydromet.* **5**, 611–624.

Andreas, E. L, Jordan, R. E. & Makshtas, A. P. 2005*a* Parameterizing turbulent exchange over sea ice: the Ice Station Weddell results. *Boundary-Layer Met.* **114**, 439–460.

Andreas, E. L, Persson, P. O. G., Jordan, R. E., Horst, T. W., Guest, P. S., Grachev, A. A. & Fairall, C. W. 2005*b* Parameterizing the turbulent surface fluxes over summer sea ice. In (CD-ROM) *8th Conf. on Polar Meteorology and Oceanography*, American Meteorological Society, 9 pp. http://ams.confex.com/ams/pdfpapers/83848.pdf.

Arya, S. P. 1988 *Introduction to Micrometeorology*. Academic.

Bendat, J. S. & Piersol, A. G. 1971 *Random Data: Analysis and Measurement Procedures*. John Wiley.

Bintanja, R. 2002 A new power-law relation for the vertical distribution of suspended matter. *Boundary-Layer Met*. **104**, 305–317.

Blackadar, A. K. & Tennekes, H. 1968 Asymptotic similarity in neutral barotropic planetary boundary layers. *J. Atmos. Sci*. **25**, 1015–1020.

Busch, N. E. 1973 On the mechanics of atmospheric turbulence. In *Workshop on Micrometeorology* (ed. D. A. Haugen), pp. 1–65. American Meteorological Society.

Busch, N. E., Christensen, O., Kristensen, L., Lading, L. & Larsen, S. E. 1980 Cups, vanes, propellers, and laser anemometers. In *Air–Sea Interaction: Instruments and Methods* (ed. F. Dobson, L. Hasse & R. Davis), pp. 11–46. Plenum Press.

Businger, J. A. 1973 Turbulent transfer in the atmospheric surface layer. In *Workshop on Micrometeorology* (ed. D. A. Haugen), pp. 67–100. American Meteorological Society.

Businger, J. A. 1982 Equations and concepts. In *Atmospheric Turbulence and Air Pollution Modelling* (ed. F. T. M. Nieuwstadt & H. van Dop), pp. 1–36. D. Reidel.

Businger, J. A., Wyngaard, J. C., Izumi, Y. & Bradley, E. F. 1971 Flux-profile relationships in the atmospheric surface layer. *J. Atmos. Sci*. **28**, 181–189.

Caughey, S. J., Wyngaard, J. C. & Kaimal, J. C. 1979 Turbulence in the evolving stable boundary layer. *J. Atmos. Sci*. **36**, 1041–1052.

Déry, S. J. & Taylor, P. A. 1996 Some aspects of the interaction of blowing snow with the atmospheric boundary layer. *Hydrol. Processes* **10**, 1345–1358.

Dyer, A. J. 1974 A review of flux–profile relationships. *Boundary-Layer Met*. **7**, 363–372.

Dyer, A. J. & Bradley, E. F. 1982 An alternative analysis of flux-gradient relationships at the 1976 ITCE. *Boundary-Layer Met*. **22**, 3–19.

Fairall, C. W., Bradley, E. F., Rogers, D. P., Edson, J. B. & Young, G. S. 1996 Bulk parameterization of air–sea fluxes for Tropical Ocean–Global Atmosphere Coupled-Ocean Atmosphere Response Experiment. *J. Geophys. Res*. **101**, 3747–3764.

Fairall, C. W., Bradley, E. F., Hare, J. E., Grachev, A. A. & Edson, J. B. 2003 Bulk parameterization of air–sea fluxes: updates and verification for the COARE algorithm. *J. Climate* **16**, 571–591.

Finkelstein, P. L. & Sims, P. F. 2001 Sampling error in eddy correlation flux measurements. *J. Geophys. Res*. **106**, 3503–3509.

Firebaugh, G. & Gibbs, J. P. 1985 User's guide to ratio variables. *Am. Sociol. Rev*. **50**, 713–722.

Fleagle, R. G. & Businger, J. A. 1980 *An Introduction to Atmospheric Physics*, 2nd edn. Academic.

Francey, R. J. & Garratt, J. R. 1981 Interpretation of flux-profile observations at ITCE (1976). *J. Appl. Met*. **20**, 603–618.

Frenzen, P. & Vogel, C. A. 1995*a* On the magnitude and apparent range of variation of the von Karman constant in the atmospheric surface layer. *Boundary-Layer Met*. **72**, 371–392.

Frenzen, P. & Vogel, C. A. 1995*b* A further note 'On the magnitude and apparent range of variation of the von Karman constant'. *Boundary-Layer Met*. **73**, 315–317.

Garratt, J. R. 1992 *The Atmospheric Boundary Layer*. Cambridge University Press.

Gill, G. C. 1973 The helicoid anemometer: a long neglected but valuable anemometer. *Atmosphere* **11**, 145–155.

Goldstein, S. (ed.) 1965 *Modern Developments in Fluid Dynamics,* vol. 1. Dover.

Gordon, A. L. & Lukin, V. V. 1992 Ice Station Weddell #1. *Antarct. J. U. S*. **27**(5), 97–99.

Grachev, A. A., Fairall, C. W., Persson, P. O. G., Andreas, E. L & Guest, P. S. 2005 Stable boundary-layer scaling regimes: the SHEBA data. *Boundary-Layer Met*. **116**, 201–235.

Guest, P. S. & Davidson, K. L. 1991 The aerodynamic roughness of different types of sea ice. *J. Geophys. Res*. **96**, 4709–4721.

Hicks, B. B. 1978*a* Comments on 'The characteristics of turbulent velocity components in the surface layer under convective conditions', by H. A. Panofsky, H. Tennekes, D. H. Lenschow, and J. C. Wyngaard. *Boundary-Layer Met*. **15**, 255–258.

Hicks, B. B. 1978*b* Some limitations of dimensional analysis and power laws. *Boundary-Layer Met*. **14**, 567–569.

Hinze, J. O. 1975 *Turbulence,* 2nd edn. McGraw–Hill.

Högström, U. 1985 Von Kármán's constant in atmospheric boundary layer flow: reevaluated. *J. Atmos. Sci.* **42**, 263–270.

Högström, U. 1986 Reply. *J. Atmos. Sci.* **43**, 2131–2134.

Högström, U. 1996 Review of some basic characteristics of the atmospheric surface layer. *Boundary-Layer Met.* **78**, 215–246.

Inoue, J. 1989 Surface drag over the snow surface of the Antarctic Plateau: 1. Factors controlling surface drag over the katabatic wind region. *J. Geophys. Res.* **94**, 2207–2217.

Intrieri, J. M., Fairall, C. W., Shupe, M. D., Persson, P. O. G., Andreas, E. L, Guest, P. S. & Moritz, R. E. 2002 An annual cycle of Arctic surface cloud forcing at SHEBA. *J. Geophys. Res.* **107**(C10), SHE 13-1–SHE 13-14. (doi: 10.1029/2000JC000439).

ISW Group 1993 Weddell Sea exploration from ice station. *Eos, Trans. Am. Geophys. Union* **74**, 121–126.

Jordan, R. E., Andreas, E. L & Makshtas, A. P. 1999 Heat budget of snow-covered sea ice at North Pole 4. *J. Geophys. Res.* **104**, 7785–7806.

Kahl, J. D. 1990 Characteristics of the low-level temperature inversion along the Alaskan Arctic coast. *Intl J. Climatol.* **10**, 537–548.

Kaimal, J. C. & Finnigan, J. J. 1994 *Atmospheric Boundary Layer Flows: Their Structure and Measurement*. Oxford University Press.

Kaimal, J. C. & Gaynor, J. E. 1991 Another look at sonic thermometry. *Boundary-Layer Met.* **56**, 401–410.

Kaimal, J. C., Wyngaard, J. C. & Haugen, D. A. 1968 Deriving power spectra from a three-component sonic anemometer. *J. Appl. Met.* **7**, 827–837.

Kaimal, J. C., Wyngaard, J. C., Izumi, Y. & Coté, O. R. 1972 Spectral characteristics of surface-layer turbulence. *Q. J. R. Met. Soc.* **98**, 563–589.

Kaimal, J. C., Gaynor, J. E., Zimmerman, H. A. & Zimmerman, G. A. 1990 Minimizing flow distortion errors in a sonic anemometer. *Boundary-Layer Met.* **53**, 103–115.

Kenney, B. C. 1982 Beware of spurious self-correlations! *Water Resour. Res.* **18**, 1041–1048.

Kondo, J. & Sato, T. 1982 The determination of the von Kármán constant. *J. Met. Soc. Japan* **60**, 461–471.

Kristensen, L. & Fitzjarrald, D. R. 1984 The effect of line averaging on scalar flux measurements with a sonic anemometer near the surface. *J. Atmos. Ocean. Technol.* **1**, 138–146.

Kristensen, L., Mann, J., Oncley, S. P. & Wyngaard, J. C. 1997 How close is close enough when measuring scalar fluxes with displaced sensors. *J. Atmos. Ocean. Technol.* **14**, 814–821.

Kronmal, R. A. 1993 Spurious correlation and the fallacy of the ratio standard revisited. *J. R. Statist. Soc.* A **156**, 379–392.

Larsen, S. E., Edson, J. B., Fairall, C. W. & Mestayer, P. G. 1993 Measurement of temperature spectra by a sonic anemometer. *J. Atmos. Ocean. Technol.* **10**, 345–354.

Long, C. E., Wiberg, P. L. & Nowell, A. R. M. 1993 Evaluation of von Karman's constant from integral flow parameters. *J. Hydraul. Engng ASCE* **119**, 1182–1190.

McKeon, B. J. 2003 High Reynolds number turbulent pipe flow. PhD thesis, Princeton University.

McKeon, B. J., Li, J., Jiang, W., Morrison, J. F. & Smits, A. J. 2004 Further observations on the mean velocity distribution in fully-developed pipe flow. *J. Fluid Mech.* **501**, 135–147.

Mahrt, L. 1998 Flux sampling errors for aircraft and towers. *J. Atmos. Ocean. Technol.* **15**, 416–429.

Margenau, H. & Murphy, G. M. 1956 *The Mathematics of Physics and Chemistry*. Van Nostrand.

Monin, A. S. & Yaglom, A. M. 1971 *Statistical Fluid Mechanics: Mechanics of Turbulence*, vol. 1. MIT Press.

Moore, C. J. 1986 Frequency response corrections for eddy correlation systems. *Boundary-Layer Met.* **37**, 17–35.

Nagib, H., Christophorou, C. & Monkewitz, P. 2004 Impact of pressure-gradient conditions on high Reynolds number turbulent boundary layers. In *XXI International Congress of Theoretical and Applied Mechanics*, International Union of Theoretical and Applied Mechanics, 2 pp. http://fluid.ippt.gov.pl/ictam04/.

Nieuwstadt, F. T. M. 1984 The turbulent structure of the stable nocturnal boundary layer. *J. Atmos. Sci.* **41**, 2202–2216.

Oncley, S. P., Friehe, C. A., Larue, J. C., Businger, J. A., Itsweire, E. C. & Chang, S. S. 1996 Surface-layer fluxes, profiles, and turbulence measurements over uniform terrain under near-neutral conditions. *J. Atmos. Sci.* **53**, 1029–1044.

Österlund, J. M., Johansson, A. V., Nagib, H. M. & Hites, M. H. 2000 A note on the overlap region in turbulent boundary layers. *Phys. Fluids* **12**, 1–4.

Overland, J. E. & Colony, R. L. 1994 Geostrophic drag coefficients for the central Arctic derived from Soviet drifting station data. *Tellus* **46**A, 75–85.

Overland, J. E. & Davidson, K. L. 1992 Geostrophic drag coefficients over sea ice. *Tellus* **44**A, 54–66.

Panofsky, H. A. & Dutton, J. A. 1984 *Atmospheric Turbulence: Models and Methods for Engineering Applications*. John Wiley.

Paulson, C. A. 1970 The mathematical representation of wind speed and temperature profiles in the unstable atmospheric surface layer. *J. Appl. Met*. **9**, 857–861.

Perovich, D. K., Tucker, W. B., III & Ligett, K. A. 2002 Aerial observations of the evolution of ice surface conditions during summer. *J. Geophys. Res.* **107**(C10), SHE 24-1–SHE 24-14. (doi: 10.1029/2000JC000449).

Perovich, D. K., Grenfell, T. C., Richter-Menge, J. A., Light, B., Tucker, W. B., III & Eicken, H. 2003 Thin and thinner: sea ice mass balance measurements during SHEBA. *J. Geophys. Res.* **108**(C3), SHE 26-1–SHE 26-21. (doi: 10.1029/2001JC001079).

Perry, A. E., Hafez, S. & Chong, M. S. 2001 A possible reinterpretation of the Princeton superpipe data. *J. Fluid Mech.* **439**, 395–401.

Persson, P. O. G., Fairall, C. W., Andreas, E. L, Guest, P. S. & Perovich, D. K. 2002 Measurements near the Atmospheric Surface Flux Group tower at SHEBA: near-surface conditions and surface energy budget. *J. Geophys. Res.* **107**(C10), SHE 21-1–SHE 21-35. (doi: 10.1029/2000JC000705).

Schlichting, H. 1968 *Boundary-Layer Theory*, 6th edn. McGraw–Hill.

Schotanus, P., Nieuwstadt, F. T. M. & De Bruin, H. A. R. 1983 Temperature measurements with a sonic anemometer and its application to heat and moisture fluxes. *Boundary-Layer Met*. **26**, 81–93.

Serreze, M. C., Kahl, J. D. & Schnell, R. C. 1992 Low-level temperature inversions of the Eurasian Arctic and comparisons with Soviet drifting station data. *J. Climate* **5**, 615–629.

Sorbjan, Z. 1989 *Structure of the Atmospheric Boundary Layer*. Prentice–Hall.

Sturm, M., Holmgren, J. & Perovich, D. K. 2002 Winter snow cover on sea ice of the Arctic Ocean at the Surface Heat Budget of the Arctic Ocean (SHEBA): temporal evolution and spatial variability. *J. Geophys. Res.* **107**(C10), SHE 23-1–SHE 23-17. (doi: 10.1029/2000JC000400).

Taylor, P. A. & Dyer, K. R. 1977 Theoretical models of flow near the bed and their implications for sediment transport. In *The Sea*, vol. 6, pp. 579–601. John Wiley.

Telford, J. W. 1982 A theoretical value for von Karman's constant. *Pure Appl. Geophys.* **120**, 648–661.

Telford, J. W. & Businger, J. A. 1986 Comment on 'Von Kármán's constant in atmospheric boundary layer flow: reevaluated'. *J. Atmos. Sci.* **43**, 2127–2130.

Tennekes, H. 1968 Outline of a second-order theory of turbulent pipe flow. *AIAA J.* **6**, 1735–1740.

Tennekes, H. 1973 The logarithmic wind profile. *J. Atmos. Sci.* **30**, 234–238.

Tennekes, H. 1982 Similarity relations, scaling laws and spectral dynamics. In *Atmospheric Turbulence and Air Pollution Modelling* (ed. F. T. M. Nieuwstadt & H. van Dop), pp. 37–68. D. Reidel.

Tennekes, H. & Lumley, J. L. 1972 *A First Course in Turbulence*. MIT Press.

Treviño, G. & Andreas, E. L 2000 Averaging intervals for spectral analysis of nonstationary turbulence. *Boundary-Layer Met*. **95**, 231–247.

Tseng, R.-S., Hsu, Y.-H. L. & Wu, J. 1992 Methods of measuring wind stress over a water surface – Discussions of displacement height and von Karman constant. *Boundary-Layer Met*. **58**, 51–68.

Uttal, T., Curry, J. A., McPhee, M. G. *et al.* 2002 Surface Heat Budget of the Arctic Ocean. *Bull. Am. Met. Soc*. **83**, 255–275.

Vogel, C. A. & Frenzen, P. 2002 On reasons for the observed variation of the von Karman constant in the atmospheric surface layer. In *15th Symp. on Boundary Layers and Turbulence*, pp. 422–423. American Meteorological Society.

Wamser, C. & Lykossov, V. N. 1995 On the friction velocity during blowing snow. *Beitr. Phys. Atmos.* **68**, 85–94.

Wieringa, J. 1980 A revaluation of the Kansas mast influence on measurements of stress and cup anemometer overspeeding. *Boundary-Layer Met.* **18**, 411–430.

Wieringa, J. 1993 Representative roughness parameters for homogeneous terrain. *Boundary-Layer Met.* **63**, 323–363.

Wyngaard, J. C. 1981 Cup, propeller, vane, and sonic anemometers in turbulence research. *Annu. Rev. Fluid Mech.* **13**, 399–423.

Wyngaard, J. C., Businger, J. A., Kaimal, J. C. & Larsen, S. E. 1982 Comments on 'A revaluation of the Kansas mast influence on measurements of stress and cup anemometer overspeeding'. *Boundary-Layer Met.* **22**, 245–250.

Yaglom, A. M. 1974 Data on turbulence characteristics in the atmospheric surface layer. *Izv. Acad. Sci. USSR, Atmos. Ocean. Phys.* **10**, 341–352.

Yaglom, A. M. 1993 Similarity laws for wall turbulent flows: their limitations and generalizations. In *New Approaches and Concepts in Turbulence* (ed. Th. Dracos & A. Tsinober), pp. 7–27. Birkhäuser.

Yakhot, V. & Orszag, S. A. 1986*a* Renormalization group analysis of turbulence. *Phys. Rev. Lett.* **57**, 1722–1724.

Yakhot, V. & Orszag, S. A. 1986*b* Renormalization group analysis of turbulence. I. Basic theory. *J. Scient. Comput.* **1**, 3–51.

Zagarola, M. V. & Smits, A. J. 1998 Mean-flow scaling of turbulent pipe flow. *J. Fluid Mech.* **373**, 33–79.

Zanoun, E.-S., Durst, F. & Nagib, H. 2003 Evaluating the law of the wall in two-dimensional fully developed turbulent channel flows. *Phys. Fluids* **15**, 3079–3089.